We thank all the reviewers for their helpful comments. We have made many revisions to the paper and have detailed our responses to all comments in blue text

Our responses to Anonymous Referee 1's comments begin on page 2

Our responses to Toshiyuki Hibiya's comments begin on page 6

Our responses to Cynthia Bluteau's comments begin on page 8

A version of the manuscript showing the changes from the previous version is appended to the end of this document.

We have made a few other changes that are not directly in response to any of the reviewers' comments.

- The quantity $\langle V_T^2 \rangle$ for each thermistor is no longer part of the transmitted dataset since $\langle V_T^2 \rangle = \langle V_T \rangle^2$ to a very good approximation, and we already have $\langle V_T \rangle$. We did not previously recognize this opportunity to further reduce the transmitted dataset.
- Instead of transmitting both $\langle V_P \rangle$ and ΔV_P for each segment, we transmit the final V_P value in each segment. The former two quantities can be derived from the final V_P values.
- The two changes above reduced the number of quantities in the transmitted dataset from 15 to 12.
- We have changed the thermal response transfer function (Appendix A) from the one discussed in Sommer et al. (2013) to one shown in Nash et al. (1999). In an earlier review, it was noted that the Sommer et al. correction is overly aggressive. In hindsight, we should have made the change then. We are making it now.
- We added a factor of H^2_{Tt}, which was missing from the expression for Φ_{Tz}

Review by anonymous reviewer

I think this is an interesting paper describing a good method, but I'm not entirely convinced that there is a great reason for doing the fits on a constant frequency band, besides the convenience. The on-board processing is already complicated enough - ultimately I don't understand why the on-board processing shouldn't be more complete (doing the fits on fixed spatial scales on the wavenumber scaled spectra?) or much simpler (by sending back a more representative voltage spectra and doing the fit on shore)?

Our scheme's on-board component involves just as many steps as the reviewer's "much simpler" approach. That is, the reviewer is suggesting we send back representative voltage spectra (presumably with some band averaging to reduce the file size). That is effectively all we are doing on board. We define two bands (1–3 and 3–5 Hz) and then do a band-averaging of sorts across each one. For shear, for example, we calculate $\sum f^{1/3} \Psi_s / \sum f^{2/3}$ (see Figure 11). This calculation is marginally more complicated than that of a mean.

Taking the "more complete" approach is much more involved as it requires calibrating the shear and temperature gradient data (and the pressure to get profiling speed). And then implementing a nonlinear curve fitting routine. All of these steps introduce possibilities for errors to creep in. Our scheme was developed to circumvent these possibilities.

Getting good estimates when the vertical velocity is not the nominal 0.2 m/s (e.g., near the top of the profiles, as the float comes to the surface) seems to be a very important aspect for the specific instrument discussed.

Yes, one of our scientific goals with FCS is to quantify turbulence in the near surface. From our 2019 experiments we learned that faster profiling is generally better near the surface; if the instrument moves too slowly, then wave orbitals introduce problems. We now note in section 3.4 that segments that are negatively affected by waves have two tell-tale signs: (i) W_{min} is not close to $\langle W \rangle$ and (ii) the fit scores are low because wave motion introduces variance at low frequencies. This causes spectra to be redder than expected and therefore they do not conform to the Nasmyth/Kraichnan models.

As far as I understand, the results are only obtained by fitting frequencies between 1 and 5 Hz. That corresponds to only 10 points in the spectrum… Separating this results on doing the fit on 5 points. Going from the full-spectrum (100 Hz for 5 sec. = 500 points) to 10 points is ultimately the core of the data reduction scheme. The paper claims that one can estimate accurate rates of dissipation from this narrow frequency range (without fancy despiking or using acceleration data). For these 10 points (for each channel), the fitting method returns 2 fitted values (factor of 5). This additional factor of 5 certainly a nice reduction. I also wonder at what precision that data is returned. Choosing a different number representation, or compression could also help here.

We have added a note in the conclusion that for a given dive:

"Transmitting each quantity as a 16-bit float or integer equates to approximately 6 kB per dive. This can be reduced by one-third if the spectral fit metrics are suitably scaled logarithmically and then transmitted as 8-bit integers."

This is our approach for future FCS deployments.

That being said, the paper is generally clear and the method is well documented. Particularly if the profiling (or horizontal velocity) varies a bit more widely, I would hesitate to really champion that method (because of the relatively narrow and fixed frequency band were the fits are done), but I can see how it might be useful and accurate for the application in question.

In section 8, we describe how our scheme could be adapted to profilers with different nominal velocities. If the chosen frequency band is suitably adapted, there's no reason our scheme cannot apply. Of course, we wouldn't recommend anyone blindly apply our scheme to a different profiler without thoroughly testing with an existing dataset from that profiler.

A few more comments:

Line 23-24: It would be useful to state the size of a typical dataset from an Argo float (one profile every 10 days). Something like "In contrast, a typical Argo profile (once every 10 days) contains XXX kB of data).

One of our goals with FCS is to profile the upper ocean rapidly—to about 120 m once every 30 minutes. Obviously, this is very different to the conventional Argo profile of 2000 m every 10 days. Hence, the comparison to the file size of a typical Argo profile is not relevant here. It is only the rate of transmission that we care about.

We have revised the Introduction to make our scientific goals, and hence our data transmission needs, more explicit.

Line 54: Why is there a 3-axis accelerometer, compass, and pitot tube? What is done with that data? In addition to the data compression, if might be worth it to discuss power consumption…

We use the accelerometer to calculate surface wave height spectra when the profiler is surfaced (though the method is detailed elsewhere).

Otherwise, accelerometer, compass, and pitot data are all recorded internally. We do this in case we can recover the profiler and obtain the full, raw dataset. These auxiliary data are useful but not essential, and so they are not transmitted in any way.

In hindsight, noting that FCS includes a compass and pitot tube does not help the reader in any way, so we have removed any description of these two sensors.

Power consumption is certainly part of our research group's discussion, but this is outside the scope of the paper. More generally, engineering details for FCS are described in a separate paper that currently has a status of Minor Revisions for *J. Atmos. Oceanic Tech.:*

Flippin' χSOLO, an Upper Ocean Autonomous Turbulence Profiling Float
J. N. Moum, D. L. Rudnick, E. L. Shroyer, K. G. Hughes, B. D. Reineman, K. Grindley, J. Sherman, P. Vutukur, C. Van Appledorn , K. Latham, A. J. Moulin and T. M. S. Johnston.

Line 148: Could horizontal velocities impact the estimate of *W*? In particular, wave motion will have some horizontal component that is not present in pressure, but does advect turbulence past the sensor, no? In other words, are there situations where the flow past the sensor is not strictly vertical?

Based on analyses not described in the paper, we have found that—to a first order approximation—FCS as a whole is advected by waves. Therefore, the flow past the sensor relative to the instrument's body is independent of wave velocities, both horizontal and vertical. Of course, this is only an approximation and there could be nonzero residual horizontal velocities. We are assuming these are small such that they would have no effect if added in quadrature to dp/dt.

More generally, we are aware that W = dp/dt is not a perfect measure of the speed of the sensors relative to the surrounding fluid. Indeed, the main reason that we include the $\langle W_{min} \rangle$ quantity in our scheme is to identify segments in which W is questionable.

L170: "two-stage approach". This phrasing, and the following sentence, made me expect that a description of the second stage would immediately follow. As it is now, I'm not sure I can readily identify the second stage (not mentioned until line 188).

We have added a sentence so that the expected parallel structure occurs. The paragraph now reads "Here we develop a new and simpler two-stage approach to fitting shear spectra to Φ_{Na}. In the first stage, …. In the second stage, …."

When the initial fit on the voltage is done on a frequency range past the inertial subrange, it seems that the least-square fit would be really dominated by the lower frequency elements of the band, since the spectrum rolls off so rapidly. The fit then doesn't really help with any noise (for example, in Fig 3b). That is presumably captured in the score.

Yes, the fit value is weighted more by the lower frequencies due to roll off, but

(1) the value of F_{Na} is also weighted more by lower frequencies and so counteracts the effect in question when it comes to calculating ε; and
(2) the roll off between 1 and 3 Hz and 3 and 5 Hz is typically small enough that the effects are limited.

Regarding point 1, consider Figure 1b, which uses one band (1–5 Hz) instead of two (1–3 and 3–5 Hz). The value of F_{Na} = 0.238 comes from an integral over 5–25 cpm. Half of the this 0.238 value comes from the first 17% of the 5–25 cpm range.

Regarding point 2, except for $\varepsilon < 10^{-9}$ W/kg, the difference in Φ_{Na} at 1 Hz and 3 Hz (nominally 5 and 15 cpm) is a factor of 5 or less. And similarly for 3 and 5 Hz. In other words, the reviewer's concern is most relevant for low ε (which makes sense because that is when the roll off will be largest). However, as we note in section 4.3, issues with low ε are less concerning to us because they "have minimal effect on any averages given that turbulence distributions have high kurtosis, so high values dominate means".

All the fits in Fig 4 have about the same value of epsilon. It might be interesting to have a column in Fig 4 for much smaller values (10^{-10}), and larger (10^{-6}, say), to see how the fit is affected by what frequency/wavenumber range it is done over…

We have changed Fig 4 so that it now has three columns with five panels per column, not one column with eight panels. The left column has examples with $\varepsilon = 10^{-9}$–10^{-8} W/kg. The middle column has $\varepsilon = 10^{-8}$–10^{-7} W/kg. The right column has $\varepsilon = 10^{-7}$–10^{-6} W/kg.

Raw data are typically not going to be recovered… What is reason for sampling so fast, if only data up to 5 Hz are used? Naively, perhaps, an analog filter could be used and microstructure signal could be sampled slower, no? Would that save power?

Although our scheme is designed so that FCS is expendable, we may still recover the instruments on occasion, in which case we prefer to have the full 100-Hz raw data available. Further, any power savings are unlikely to be worth the effort of redesigning the existing circuits.

Review by Toshiyuki Hibiya

Summary

Considering that continuous turbulence observations using autonomous and expendable profiling floats such as Deep Argo floats will be the norm in the near future, the development of the data reduction scheme as described in this paper is indispensable and deserves publication. Nevertheless, I am still not convinced about some aspects of the data reduction scheme described in the paper, so that I would be happy to receive some answers before publication.

Thank you for the review.

Major Comment

1. The data reduction scheme proposed in this paper presupposes the existence of a spectral slope with $k^{1/3}$ dependence in the inertial subrange. However, Figure 4 shows that the shape of the measured shear spectrum significantly deviates from that of the Nasmyth spectrum, and does not appear to have the $k^{1/3}$ slope presupposed in the inertial subrange. I am afraid that, in this case, the proposed formulation to obtain ε using the correction factor F_{Na} defined by (17) and (20) might break down.

Our scheme does not presuppose that measured spectra have $k^{1/3}$ slopes. Yes, a $k^{1/3}$ slope is initially assumed but, as we note in the paper:

"Our inertial subrange assumption is often false. Indeed, 'assumption' is perhaps a misnomer as we do not expect it to be true; we know that viscous roll off will often occur at frequencies lower than 5 Hz (25 cpm for a nominal value of W = 0.2 m/s)."

The statement above is key to understanding our unorthodox approach to calculating ε. However, it is buried somewhat in the middle of section 4.1. Therefore, we have added the following paragraph right at the beginning of section 4 to alert the reader to this point:

"In this section, we are ultimately going to fit measured spectra to an inertial subrange model that does not necessarily apply at the relevant frequencies or wavenumbers. We will elaborate as we go, but we want to emphasize in advance that measured spectra do not need to conform to an inertial subrange model for us to obtain accurate values of ε. The inertial subrange is merely a convenient starting point."

Perhaps the best evidence that F_{Na} and hence ε is correct is the agreement between ε from the reduced scheme and that from our standard processing (Figs 5 and 6).

2. Also, in this case, does the "fit score" defined in this study have any meaning? In other words, even if a good fit score is obtained by matching the ε calculated for 1-3 Hz with that for 3-5 Hz, this cannot necessarily be an indicator of a good match between the measured spectrum and the Nasmyth spectrum, and it may cause errors in the estimation of ε using (17) and (20), right?

The fit score is simply the ratio of two independent values of ε: one from 1–3 Hz and one from 3–5 Hz. Each of these are derived from their respective values of ε_{init} and F_{Na}. As shown in Figure 3a, the two dark blue lines match up, which is equivalent to saying that the two ε values match. These lines match up because the original measured spectrum (brown line) looks like a Nasmyth spectrum. The opposite is

true for Figures 3b and 3c—the dark blue lines don't match—because the measured spectra don't match well with the Nasmyth spectrum. So, yes, a high fit score does provide an indicator of a good match between the measured spectrum and the Nasmyth spectrum.

3. In section 4.1, the method for obtaining ε_{init} is not presented, and the discussion in section 4.1 proceeds without clarifying the definition of ε_{init}. Wouldn't it be easier to understand the overall flow of the discussion if the definition of ε_{init} written in section 4.2 were given first, followed by the discussion in section 4.1?

The original text did define ε_{init} but it was an implicit definition and hidden somewhat in the middle of a paragraph. We have reworded a few paragraphs in section 4.1 to highlight the definition of ε_{init} and point the reader to the fitting method in Appendix C.

4. Please add to the end of section 7 the reason why the agreement between the obtained χ values and those obtained from the standard scheme becomes worse than in the case of ε, even though the method for obtaining χ from the reduced scheme is basically the same as in the case of ε.

We have added the following paragraph:

"There are three reasons for the poorer fits to temperature gradient spectra compared to that for shear. First, shapes of temperature gradient spectra are often more variable; the best choice for non-dimensional spectral model can be debated (e.g., Sanchez et al. 2011). Second, the temperature gradient fits depend on ε. Uncertainties in ε propagate into the calculation of χ. Third, for our 2019 experiment, the recorded temperature gradient signals"

Minor comments

5. Line 198: six times smaller than → eight times smaller than

Good catch. Changed as suggested.

6. Although $H_s(k)$ is defined in (3), it appears somewhat suddenly in (19) in section 4.1 without any connection to the preceding discussion, which seems a bit awkward.

We have re-ordered the text to get rid of the awkwardness. Previously, the two forms of F_{Na} were defined in Eqs 18 and 20, with the awkward discussion of H_s^2 in between. Now, the two forms are given in Eqs 18 and 19 and H_s^2 is discussed in its own paragraph afterwards.

7. Just below color tones in Figures 7 and 10: proportion (%) → proportion (× 100 %)

The label is correct as is. There are many hundreds of nonzero bins in these 2D histograms and the upper limit of the colour axes are <1%.

Review by Cynthia Bluteau

Summary

I initially refused the review request but can now provide comments. I've elected to do so as a community member rather than an anonymous reviewer. My review will be more narrated than usual, given the open peer discussion at EGU journals. My understanding is the authors developed a "reduced algorithm" for estimating two turbulence quantities (ε and χ) from the voltage spectra of shear and fast-temperature sensors onboard an expendable profiler (SOLO). It needs to be clarified from the methods' description, but the χ estimates rely on first obtaining ε from the shear probe. The algorithms are designed to minimize the data transfer rate by fitting a narrow range of frequencies of voltage spectra with a power relationship. This model spectra may not apply over the fitted range (as noted by the authors). Whether the observations are expected to have a power relationship over the fitted frequencies is accounted for with a correction factor F_{Na} (shear) or F_{Kr} (temperature-gradient). They have chosen the empirical Nasmyth (inertial subrange) and the Kraichnan models (viscous-convective subrange) instead of using an inertial model for both datasets or a viscous model for both. Below I summarized further my understanding of the algorithm before providing more details about modifications that may render the article more transparent for readers.

Algorithm summary

For each segment of data (e.g., ~5 s chunk of the full profile), the algorithm estimates:

- an average and minimum drop-speed onboard the instrument
- voltage frequency spectra from each temperature and shear probe sensor (are there 2x of each onboard?)
    - Their spectra have roughly 6-10 degrees of freedom in their setup by using 3 overlapping segments of 256 samples each. The spectral bandwidth is from ~0.4 Hz to 50 Hz with a frequency resolution of 0.4 Hz. The drop speed is about 0.2m/s, so their spectra cover wavenumbers ranging from 2 to 250 cpm. Given the thermal frequency response and the spatial size of the shear probe, the spectra are probably "usable" up to 20 Hz (thermistor) and 100 cpm for the shear probe. Of course, noise can limit this further. Still, the drop speed of 0.2m/s nicely "optimizes" the usable range in both the shear and temperature gradient spectra.
    - The calibration coefficients are not stored on the SOLO, unlike recoverable turbulence profilers or most ocean sensors. The lack of calibration constants prevents them from converting the voltage spectra into physical units onboard the SOLO (or onshore since no spectral observations are transmitted).
- Two power fits are performed for each voltage spectrum over a narrow bandwidth of available spectral observations. This bandwidth is between 1 and 5 Hz (1/2 decade of data). The first power fit is between 1 and 3 Hz, and the second is from 3 to 5 Hz. Overall, their 1/2 decade has 10 spectral samples, and each power fit is done with 5 samples.
- Two quantities, one for each power fit, are returned to shore for each voltage spectrum. These quantities are then converted into initial ε_{init} and χ_{init} estimates via the calibration constants of the sensors.

- From these initial estimates, the correction factors F_{Na} and F_{Kr} are used to obtain ε and χ. I presume that ε is also fed into F_{Kr} to obtain χ (not clear from the methods' description). Both correction factors depend on the frequencies fitted, the choice of model, etc. It's unclear whether F_{Na} and F_{Kr} are sufficiently general such that any frequencies could be used for fitting the voltage spectra (e.g., different profiling speed or source of vibrations).
- There are accelerometers onboard the SOLO, but they are not used to correct the turbulence (voltage) spectra. Instead, the analysis utilizes data between 1 to 5Hz to avoid surface waves and motion-contamination. The authors state the accelerometers are for computing wave statistics, which I presume will involve additional spectral computations onboard the SOLO. How the turbulence analysis changes in wavy flows dominated by surface waves should be discussed in the ms.

Thank you for providing these summaries of the paper and algorithm. A few clarifications/notes (but mostly leaving our detailed replies to the comments below):

- Yes, there are two shear sensors and two fast thermistors as noted in the second paragraph of section 2.
- We agree that the spectra are "probably useable" up to 20 Hz and 100 cpm, and less if noise is an issue. The operative word here is "probably". Our scheme is necessarily conservative about the upper limits we use for fitting. We need to be confident that the spectra that we are fitting are *useable*, not just *probably useable.* We do not have the luxury of re-examining the raw data or full spectra after they are reduced.
- Our choice to not apply calibration coefficients onboard the instrument is a feature, not a bug, if you will. We do not dwell much on this point in the paper, but postponing calibration has a big benefit: it removes the possibility of an inadvertent mistake (say, the wrong shear probe is installed, or the wrong header is applied) that would cascade through the turbulence profiling algorithm and lead to values of ε or χ that are difficult or impossible to later correct for.
- Yes, values of ε are fed into the calculation of F_{Kr}. We have added a sentence to the first paragraph of section 6 to make this clearer.
- The comment about whether F_{Na} and F_{Kr} are sufficiently general is already addressed in section 8.1 in which we provide recommendations for porting our scheme to a different profiler. In short, our scheme is suitable for different profiling speeds but it does assume that any vibrations that occur are outside the fixed frequency fitting range.
- The wave statistics do indeed involve additional spectral computations. On the advice from an early reviewer, these tangential details are left out of the paper.
- See our response to comments 7 and 8 regarding accelerometers and surface wave frequencies.

Major comments

I have grouped my concerns into three themes. The main suggestions for implementation in the ms are numbered and shown in italic purple.

1. More transparency is required in discussing the drawbacks of their chosen strategy. The algorithm was designed to limit data transmission at all costs by relying on a small subset of data recorded by the profiler.
2. Lack of assessment of the fit-score as an alternative measure of data quality.

3. Lack of transparency about the χ methods and the data quality both in applying the reduced algorithm and for estimating χ from standard practices.

1 Reduced algorithm's "framework"

1.1 Improvement over using band-averaged (low-resolution) spectra

The ms should be more transparent in explaining the drawbacks of their chosen strategy when compared to that employed by Rainville et al. (2017). As noted by the authors on L27-31, the reduced algorithms of Rainville et al. (2017) sends band-averaged (i.e., low-resolution) spectra ashore. In their case, 12 spectral observations are transmitted that cover all available lengths and timescales of turbulence, including the noise (a bit overkill, in my opinion). Specifically, their instrument sends 9 spectral samples between 2 to 100 cpm and 4 samples over the wavenumber range (5 to 25cpm) used in the current ms for fitting. The main advantage of sending spectral observations ashore is being free to apply standard fitting or integrating techniques to estimate the turbulence quantities of interest. More importantly, quality-control criteria, such as the mean absolute deviation listed by the authors on L240 can be calculated. This criterion indicates whether the observations follow the expected forms of turbulence, i.e., spectra aren't drowned by noise, motion contamination, or anisotropy. These issues are usually also nicely spotted by inspecting spectra, but with the proposed reduced algorithm in the ms, this information is lost during transmission.

1. Since the authors only used limited range of turbulence scales (1 to 5Hz), it would be worth highlighting the data "savings" that they gain by transmitting two power fit estimates (1-3Hz, and 3 to 5Hz) over sending for example 4x (band-averaged) spectral observations.

We have added details to the second paragraph of the Introduction about why Rainville et al.'s scheme is too data intensive for our purposes. In short, with two shear probes, two thermistors, and 12-element spectra, we have 48 values per segment (plus a few other quantities) that must be sent back to shore. For our profiling scenario, we'd end up spending as much time at the surface transmitting data as actually measuring the ocean. This goes against one of our scientific goals of profiling as frequently as possible.

We developed our scheme with an aim of having the smallest possible file size for transmission. That meant we used only two fitting bands (1–3 and 3–5 Hz). But there is nothing to stop someone from using our scheme with three or more fitting bands (say, adding a 5–7 Hz band) and benefiting from any improvements that this entails. We have added this recommendation to our list in section 8.1. We also note in this section that there is a point at which if the number of bands to be used is many more than two, then (as the reviewer alludes) one might as well use the Rainville et al. (2017) instead.

2. It would also be useful to say why a data reduction scheme that reduces 512 samples to 12 samples (band-averaged spectra) is inadequate, which ultimately resulted in developing an algorithm that fits a narrow range of information onboard the processor.

As in our reply above, using 12 samples per spectra leads to file sizes sufficiently large that they interfere with and limit our intended profiling strategy.

1.2 Using a limited range of frequencies for fitting

The algorithm appears highly dependent and applicable for their particular drop speed, sampling rates and frequencies used for fitting. It also depends on there being no motion contamination over the range

of frequencies used. It makes the paper highly specific for their platform, as opposed to being a "reduced algorithm" for turbulence profilers. This is fine but worth highlighting. However, the reliance on a small subset of the available turbulence information is problematic. Makes you question why even sample the shear signal at rates above 32-64Hz if we can get away with deriving ε (or χ) from such a narrow range of turbulence length/time scales.

We disagree that the scheme is “highly specific” to our platform. Section 8.1 outlines how it can be adapted for other scenarios. Nevertheless, we agree that we had not highlighted enough the assumption of no motion contamination. We now state in the abstract that “..., we focus on a fixed frequency band that we know to be unaffected by vibrations and that approximately corresponds to a wavenumber band of 5–25 cpm.”

The reviewer is correct that ε and χ from our reduced scheme would barely change if we had a sampling frequency of 32 or 64 Hz instead of 100 Hz. At the same time, we don't claim that our values of ε and χ are as exact as they could be. Nor are we suggesting that anyone should use our reduced method if they have the luxury of having raw data at 100 Hz or more. But it shouldn't be a surprise that we can get good results using a narrow frequency band. Although a wider band allows for better statistics (as the reviewer notes elsewhere in this review), this doesn't change the fact that shear spectra scale monotonically with ε. And the same for temperature gradient spectra vs χ (provided ε is known).

As a contrived example, consider a scenario in which measured spectra conform perfectly to the Nasmyth spectrum. In this case, one could calculate ε with just one coefficient from the measured spectra (in other words, a very narrow band)

Furthermore, the narrow band of scales used comprises a low number of spectral observations (5x per fit), which have low statistical significance given how the voltage spectra are calculated. The spectra use 3x FFTs with a 50% overlap, each having 256 samples, which is less than typical when accelerometers are used to decontaminate the spectra. Depending on the widowing function applied, this is about 6 to 10 degrees of freedom – a tad more than spectra with no statistical significance. The degrees of freedom wouldn’t allow using squared-coherency to decontaminate the spectra (a minimum of 7 NFFTs would be more appropriate). There’s all this effort to reduce the data transfer, but an easy saving would be using a statistically significant spectral averaging strategy, e.g., 768 samples for each segment instead of 512 samples (the 5x NFFTs would still have the exact resolution).

Turbulence processing always comes with trade-offs as the reviewer alludes. Yes, we could increase the sampling period and use more subsegments to increase statistical significance, but we then lose vertical resolution. For us, going from 512 to 768 samples equates approximately to Δz from 1.0 m to 1.5 m. These may not sound like much, but it matters a lot in places like the near-surface ocean where ε depends strongly on z.

Section 8.1 explicitly notes that N_{seg} = 512 and N_{fft} = 256 is merely the choice we made for our own scientific goals. Someone else could easily use our scheme with, say, N_{seg} = 1024 and N_{fft} = 256 to have 7 half-overlapping subsegments per segment.

3. Would the results be similar if a more statistically significant spectra were used in the calculation? Would band-averaging the spectra change the estimated ε_{init} (χ_{init})?

In the paper with N_{seg} = 512 and N_{fft} = 256, we find that the reduced scheme and standard processing agree within a factor of 2 in 87% of cases for ε and 78% of cases for χ. These became 88% and 78% when we reran the analysis with N_{seg} = 1024 (i.e., 7 subsegments rather than 3). In other words, effectively no improvement. This indicates that statistical significance of spectra is not a limiting factor on the quality of the final dataset.

4. Fig 3: Include the kinematic viscosity and confidence intervals for these spectra (see §5.4.8 Emery and Thomson, 2001) for calculating the confidence levels

If we understand correctly, the reviewer is suggesting that we add confidence intervals to the 10 spectral values in each panel. We have not done this as we think it could cause confusion. Figure 3 demonstrates visually how to calculate the ε fit score, which is a value that is independent of confidence intervals. If we include confidence intervals, the reader might incorrectly infer that confidence intervals somehow enter the fit score calculation.

Kinematic viscosity is now noted in the caption.

1.3 Number of samples used for each fit

Recent work has concluded that for data with low variance, 8 samples are required for regressions (Jenkins and Quintana-Ascencio, 2020). For highly variable datasets, this number increases to 25. The authors have used 5x spectral observations, compounding the above issue of relying on low bandwidth of turbulence spectral observations that each have low statistical significance. It makes you wonder if the least-square power fit is just a guesstimate of what the turbulence level in the signal might be.

The Jenkins and Quintana-Ascencio results have been quoted without context and they are not relevant here. The numbers 8 and 25 are for their specific and contrived scenario of distinguishing between null, linear, and quadratic data. We are doing something quite different: we have a known model to fit against and we are finding the fit coefficient. We are not trying to distinguish between models.

5. How large are the confidence intervals for the fitted quantity in Eq 23? Least-square fitting usually allows for this result to be calculated, but these have not been presented.

As we note in section 4.3, we cannot calculate conventional goodness of fit metrics (including confidence intervals for least-squares fits) with our reduced scheme because we do not know the scaling for each model spectrum until we calculate ε values in the post-processing stage. By this stage, we have lost information about the spectral shape through the summing operation in Eq. (24).

6. What would be the confidence level for ε_{init} if the spectral confidence levels were propagated, along with the errors associated with using only 5x samples for a least-square fit? The error would propagate through to F_{Na} in Fig 2.

As per our response to comment 3, we find that statistical significance of the measured spectra is not a limiting factor. And per our response to comment 5, we cannot calculate confidence intervals because we don't know ε until post-processing.

We don't mean to downplay the value of calculating uncertainties for each spectral fit, and we recognize that the reviewer has done a lot of work to help the turbulence community follow best practices on this topic. However, with a tool like FCS, we gain the luxury of a dataset with ~50 profiles per day. Hence, we

personally are better served by using bootstrapping to calculate uncertainties from repeated samples of ε and χ than we are diagnosing the confidence intervals for each individual fit.

1.4 No reduction of vibration and wave-contamination

The ms mentioned using accelerometers to determine the wave climate, so spectra are presumably being calculated. It seems no information gained from the accelerometers will be used to assess the quality of the turbulence measurements? Rather than decontaminate the shear spectra, the fit is restricted to frequencies 1 to 5Hz when some platforms do have contamination across those ranges (Fig 5 of Bluteau et al., 2016). Surface waves "seas" are awfully close to the frequency range used here.

7. The authors should acknowledge that their chosen frequencies avoids motion-contamination for their specific platform.

As noted earlier, we now state up front in the abstract that the frequency band we use is one that we know to be unaffected by vibration.

8. It would help to detail in the ms why it's unfeasible to perform this calculation onboard the processor. A squared-coherency estimate (Zhang and Moum, 2010) is mostly rearranging cross-spectral terms (conjugates of FFTs). It is not restricted to being done in physical units. This additional processing could indeed be accommodated by using longer segments. We often live with ADCP profiles with 10 m bins, so getting a lower vertical resolution turbulence signal might be worthwhile if the estimates are more robust.

On the low frequency side, decontamination via squared coherency is not going to help. The motions that we'd being trying to account for would be surface gravity waves, but the nonlinear relationship between shear and profiling speed makes this too challenging. We now note this in section 3.3. In that same section, we also now note that segments that are adversely affected by waves can be identified in post processing because they typically share two traits: $\langle W \rangle$ is not close to W_{min} and ε fit score << 1. We state that these segments should be discarded.

For f > 5 Hz, we agree that vibration decontamination is possible and that it can be done in voltage units. But, as the reviewer noted earlier, this requires ≥7 subsegments. To us, this represents too large of a constraint on the vertical resolution. We have added an explicit statement to the end of section 3.1 that we are not pursuing the possibility of motion decontamination.

2 Fit-score as a quality-control indicator

The authors' "fit-score" is the ratio of the result obtained using the first 5 samples (1 to 3 Hz) vs the subsequent 5 samples (3 to 5Hz). This quantity tests crudely the sensitivity of the results to a very slight change in frequencies. Having used it myself as a qualitative guide (see Fig 4 of Bluteau et al., 2011), I'm concerned that there's no measure of whether the entire spectra are "garbage" particularly the temperature gradient spectra that are usually much more variable in quality.

If the turbulence shape varies widely over such small changes in frequencies, then, indeed, the data is very poor. The question, though, becomes, how poor? How much variations in shape can we expect? Does this variation depend on the spectral averaging, i.e., the statistical significance of the spectra? Will the fit-score depend on the number of samples used in the individual fits? How do all of these factors translate into rejection criteria? It needs to be clarified if a rejection threshold was proposed. What's

evident in the manuscript is that the fit-score it's now the primary way to assess quality, given that the reduced algorithm does not send spectra observations to shore.

9. To develop and assess the algorithm, the SOLO was recovered. Thus, it's possible to estimate the mean absolute deviation listed on L240. The mad has existed for 22 years and is on its way to being recommended by the SCOR working group #160 as a quality-control indicator for data archiving. The fit-score should be compared to the mean absolute deviation (mad) for all segments in a scatter plot. The scatter plot would enable readers to judge the robustness and usefulness of the fit-score as a quality-control indicator. Let the data speak for itself.

Although our fit score and the mean absolute deviation are both goodness of fit measures, they quantify different aspects and there is not an apples-to-apples comparison between the two.

- Mean absolute deviation, as its name implies, focuses on the size of the residuals.
- Our fit score is more focused on whether the residuals are random or autocorrelated.

We have added three sentences to section 4.3 explaining that our fit score focuses on random vs autocorrelated residuals.

To elaborate, consider the spectra examples in Figure 4. Those with the higher scores tend to have unbiased residuals: measured spectral coefficients are just as likely to be above the fit as below it. Those with lower scores tend to have autocorrelated residuals (often manifesting as the sign of the residuals being a function of frequency). Take, for example, a spectrum from Figure 4 whose fit score is low because all coefficients with $f < 3.3$ Hz have negative residuals and vice versa:

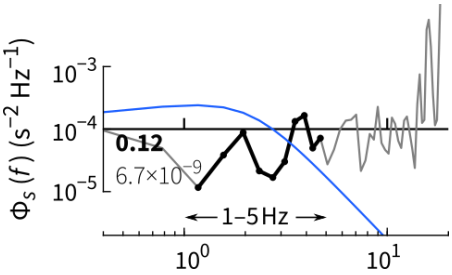

This example would also have a large MAD because it's a poor fit full stop. But there are cases where the MAD is large (→ bad fit) but the fit scores are close to 1 (→ good fit) because the residuals are large but not autocorrelated.

Obviously, we prefer that our fits don't have large residuals, but the more pressing concern is that the fits do not have autocorrelated residuals.

For what it is worth, we did do the comparison of **

(1) ε fit score vs MAD($\Phi_s/\Phi_{Na} - \langle\Phi_s/\Phi_{Na}\rangle$) over 1–5 Hz
(2) χ fit score vs MAD($\Phi_{Tz}/\Phi_{Kr} - \langle\Phi_{Tz}/\Phi_{Kr}\rangle$) over 1–5 Hz

The two quantities are clearly correlated (see figure below), but there is variability for the reasons described above.

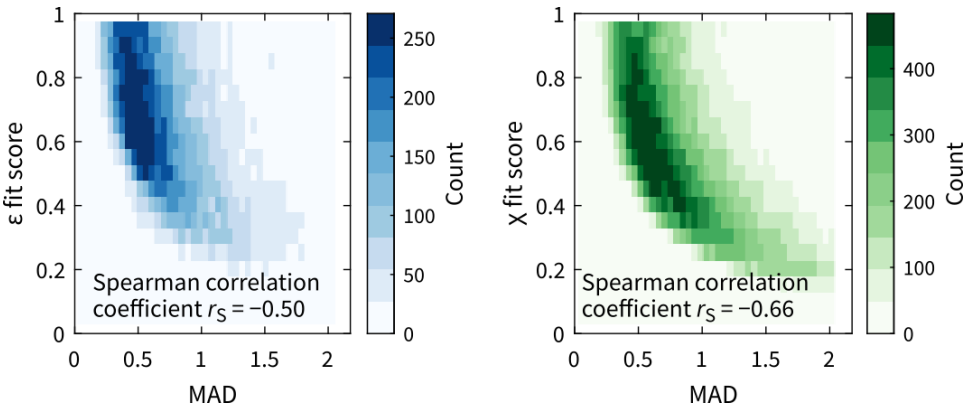

**For each fit, we actually calculated the MAD for Φ_s/Φ_{Na} and its inverse Φ_s/Φ_{Na} and took the larger MAD of the two (and similarly for Φ_{Tz}/Φ_{Kr}). We did this because there are times when Φ_s/Φ_{Na} is small because Φ_{Na} is large, not because the residuals are small. As a contrived example, $MAD(\Phi_s/\Phi_{Na} - \langle\Phi_s/\Phi_{Na}\rangle) = 0$ if Φ_s is 0 for every frequency.

3 Data quality of the temperature gradient data

3.1 Methods description

In general, the χ description is unclear. The ms is organized as if the χ estimates are done in isolation of ε, when Eq 30-31 shows that ε is required to estimate χ. This strategy differs from the many previous chipod papers (e.g., Moum and Nash, 2009; Becherer and Moum, 2017), which use the fast-temperature data to solve for both ε and χ by equating Osborn to Osborn-Cox's model. The proposed algorithm design in the ms was justified by referring to chipod papers pioneered by their research group (Becherer and Moum, 2017). However, the authors haven't highlighted that the new algorithm depends on getting ε first from the shear probe before obtaining χ from the temperature gradient spectra rather than obtaining ε and χ simultaneously from the temperature gradient spectra. Needing both shear probes and fast-temperature sensors in itself increases the amount of data processing and data transmission from the SOLO. Why not get rid of the shear probes completely? Does the SOLO not measure background temperature and salinity?

Inferring values of ε from χ is only possible where there is stratification. Since FCS is an instrument focused on the upper ocean, it will spend a lot of its time in the mixed layer. To measure ε here, it needs shear probes. We now mention this need for shear probes near the end of section 2.

10. Please explain in the intro [L35-40] whether they are using the shear probe to derive ε, and if this quantity is then used for estimating χ. Some comments as to why this strategy was chosen should be provided given it increases the demands on data processing and data transfer.

We now state in the last paragraph of the Introduction that, yes, we get ε from the shear probes and subsequently invoke this in the calculation of χ. (This is also reiterated at the start of section 6.) As the reviewer rightly notes, this is different from the chipod method. Consequently, we caused confusion by stating that we were closely following the chipod paper of Becherer and Moum (2017). We have moved and reworded the reference to Becherer and Moum so that it no longer causes confusion.

11. The ms could also better discuss the implications of relying on ε from the reduced algorithm on the quality of the χ estimates. Unless of course, they've estimated ε and χ simultaneously from the temperature gradient spectra in which case the ms should illustrate how ε_χ compares to ε obtained from the shear probes.

We have added the following paragraph to section 7 (Testing the reduction scheme for χ)

"There are three reasons for the poorer fits to temperature gradient spectra compared to that for shear. First, shapes of temperature gradient spectra are often more variable; the best choice for non-dimensional spectral model can be debated (e.g., Sanchez et al. 2011). Second, the temperature gradient fits depend on ε. Uncertainties in ε propagate into the calculation of χ. Third, for our 2019 experiment, the recorded temperature gradient signals"

We briefly reiterate this point in section 8.2

"Recall, also, that all uncertainty in ε propagates into the calculation of χ (Sect. 7). If ε for a given segment cannot be trusted, neither can χ."

12. Also re-iterate the dependency of χ on ε when presenting Eq 30-31, and on L306 when claiming the temperature gradient spectra Φ_{Kr} depends only on χ, which isn't true (see Fig r1).

The text already includes a reminder of this dependence after Equation 30.

We assume the reviewer meant line 307? This line states that $\Phi_{Kr} \propto \chi$, but it does not state it depends *only* on χ. The additional dependence on ε is already clearly stated in the definition of Φ_{Kr} in Eqs 27–28.

3.2 Information about the chi data quality

The fact that no temperature gradient spectra were shown in the ms is disconcerting. A few shear probe examples focus on observations between 1 and 5 Hz, which mask any spectral contributions from waves or motion contamination. The only spectral information for χ is the data density plots in Fig 10, which only show observations between 1 and 5Hz. Still, this figure gives an inkling of the temperature gradient data quality. Fig 10b shows a cloud of data with the wrong slope sign at non-dimensional $k \lesssim 3 \times 10^{-2}$, which then starts to fall off too early. Is this because of problems with the estimated ε shifting the spectra to the left? Fig 10c looks like spectra drowned by noise (perhaps high ε and low χ). Even the high-score examples in Fig 10a could be better. The "peak" data density doesn't fit the Kraichnan form. There's no curvature in the location of maximum data density, unlike Fig 7a for the shear probe.

I'm questioning whether it's the algorithm behaving poorly or whether the collected temperature gradient data could be of better quality at the outset.

13. To alleviate concerns about the data quality, I strongly recommend adding an extra column in Fig 7 and 10 showing the data density for all wavenumbers, not just those used by the algorithm.

As suggested, we have added the extra columns to Fig 7 and 10. The new column in Fig 7 shows that, provided the fit score $\gtrsim 0.33$, the measurements agree with the Nasmyth spectrum at all but the highest frequencies where noise becomes an issue. Conversely, the new column in Fig 10 shows looser agreement and that the effects of noise are larger. This implies that the quality of our results is not limited by the algorithm, but by the quality of the temperature gradient data.

14. Another request is adding an extra column in Fig 4 with the temperature gradient spectra collected concurrently with the shear probe. Preferably all available wavenumbers for data transparency. There are none in the ms, which masks the data quality.

The purpose of Fig 4 is *not* to demonstrate data quality. It is to demonstrate how well the ε fit score differentiates better and worse fits. We designed the figure to make it easy to follow: the fits get progressively worse moving from top to bottom. Adding a column with the concurrent temperature gradient spectra would confuse the figure as this extra column of fits would not necessarily get progressively worse in the same way.

The temperature gradient spectra certainly are of poorer quality in terms of how well they match the model form. This is now clear from the extra column added to Fig 10 as suggested in the previous comment (and discussed at the end of section 7).

15. Specify which χ estimates were rejected from the paper. Fig 10 shows variable fit-score, but which would be flagged as unusable for further analysis in a scientific article?

We now note in section 8.2 that we recommend discarding ε and χ values if their associated fit scores are less than 0.33. As with any turbulence dataset, it is always a challenge to turn a goodness-of-fit continuum into a pass/fail binary. That said, based on our analyses, we find that 0.33 is a good threshold.

16. Why use the inertial subrange model for shear but then assume the viscous-convective subrange model for temperature when the same frequencies are fitted onboard the processor? Does it not matter that the fitted model isn't expected over the range k?

There are two subranges for shear (inertial and viscous) and three for temperature gradient (inertial–convective, viscous–convective, and viscous–diffusive). We think the reviewer is implying that we use the viscous subrange for shear so that the two models are more similar? This is not obvious since there isn't a one-to-one correspondence between subranges for shear and temperature gradient.

For our scheme to work, the models used (Φ_{Na} and Φ_{Kr}) only need to have a subrange in which they are proportional to k^n (or equivalently f^n). For shear, we have $k^{1/3}$. For temperature gradient, we have k^1. These power law approximations are what makes the onboard component of the scheme simple (see sections 4.2 and 6.2).

To answer the second question in the comment, no it doesn't matter. For elaboration, see our response to the first comment by reviewer Toshiyuki Hibiya.

17. Also, please use a colour scale/scheme that compares the temperature and shear spectra data density against each other. The colour gradient presents a data count (or proportion of data), but the scheme changes between figures. If a colour theme for shear and temperature is necessary, decorate the x and y-axis colours, but leave the colour gradient the same across all the data density plots (Fig 6, 7 and 8-9).

We fail to see the reasoning behind using a single colourmap. There is never a need to compare proportions across different figures. Proportions are only meaningful within a single figure.

We use blue for shear and green for temperature gradient throughout the paper to help signal to the reader when the discussion shifts from one quantity to the other.

18. The colours in Fig 6, 7 and 8-9 also seem to saturate at values below the maximum, which makes it hard to see where the maximum sits relative to the theoretical shape (Fig 7-10) and the 1:1 slope (Fig 6 and 9). Perhaps visit brewermap or cmocean color palettes described in Thyng et al. (2016) article about ocean data visualization.

We have fixed the colour limits for the affected figures so that they no longer saturate.

Colorbrewer is the tool (via a Matlab wrapper) that we used to generate the blue and green colourmaps used in this paper.

Other comments

Misciting

Remove the erroneous citations to my published work. On L342, the reference to my article on fitting shear probe data does not state that centring a fit around 10-20 cpm minimizes sensitivity to the fitted range. The only thing that reduces this sensitivity is fitting the correct model (e.g., inertial subrange) over the wavenumbers that this model is expected to be valid. Another way to limit sensitivity is to have high-quality measurements that aren't drowned by noise, vibrations and surface waves. The range of wavenumbers would depend on data quality, drop speed, and model used for fitting. If my results were insensitive to the 10-20 cpm range, I was using a model that covered both the inertial and viscous subranges, and the data was of good quality after decontamination.

We have removed the statement in question.

L344-349. I'd remove the whole paragraph. First, the power fit used by the authors sometimes uses frequencies in the inertial subrange (1 to 5Hz translates to 5 to 25cpm). With the 0.2m/s drop speed, the inertial subrange is only being fitted with the correct model when $\varepsilon > 10^{-7}$ W kg^{-1}. For low $\varepsilon < 10^{-7}$ W/kg, the inertial subrange model is fitted to the shear probe's viscous subrange. A similar argument would apply for temperature, except that the authors have chosen to always apply the viscous-convective model instead of the inertial-convective model (Fig. r1).

We have removed the whole paragraph as suggested.

Using a moored platform changes very little other than we have to contend with variable speeds past the sensor. A mooring doesn't automatically translate into long FFT segments. My miscited article (Bluteau et al., 2011) refers to the spectral fitting of the inertial subrange of acoustic-velocity measurements – not shear probes. We use long segments because we're relying on the lower scales of turbulence since the data quality is typically too poor over the viscous subranges (technological issue). Another reason for using long segments is calculating other turbulence quantities such as Re stresses and TKE. These estimates rely on covariances and thus the integration of cospectra with reasonable statistical significance (need more NFFTs, and/or band-averaging).

The reference to Bluteau et al. (2011) was, as we noted, tangential to the paper. We see how it could cause confusion and so have removed it per the previous comment.

A turbulence data reduction scheme for autonomous and expendable profiling floats

Kenneth G. Hughes[1], James N. Moum[1], and Daniel L. Rudnick[2]

[1]College of Earth, Ocean, and Atmospheric Sciences, Oregon State University, Corvallis, Oregon.
[2]Scripps Institution of Oceanography, University of California, San Diego, La Jolla, California.

Correspondence: Kenneth Hughes (kenneth.hughes@oregonstate.edu)

Abstract. Autonomous and expendable profiling float arrays such as deployed in the Argo Program require the transmission of reliable data from remote sites. However, existing satellite data transfer rates preclude complete transmission of rapidly sampled turbulence measurements. It is therefore necessary to reduce turbulence data onboard. Here we propose a scheme for onboard data reduction and test it with existing turbulence data obtained with a ~~newly developed version of a~~ modified SOLO-II profiling float. ~~The scheme invokes simple power law fits to (i) shear probe~~ First, voltage spectra are derived from shear probe and ~~(ii)~~ fast thermistor ~~voltage spectra~~ signals. Then, we focus on a fixed frequency band that ~~yield~~ we know to be unaffected by vibrations and that approximately corresponds to a ~~fit value plus a quality control metric~~wavenumber band of 5–25 cpm. ~~At~~ Over the fixed frequency band, we make simple power law fits that—after calibration and correction in post-processing—yield values for the turbulent kinetic energy dissipation rate ε and thermal variance dissipation rate χ. With roughly 1 m vertical ~~interval resolution~~segments, this scheme reduces the necessary data transfer volume ~~240-fold~~ 300-fold to approximately ~~3~~2.5 kB for every 100 m of a profile (when profiling at 0.2 m s^{-1}). ~~Turbulent kinetic energy dissipation rate ε and thermal variance dissipation rate χ are recovered in post-processing.~~ As a test, we apply our scheme to a dataset comprising 650 profiles and compare its output to that from our standard turbulence processing algorithm. For ε, values from the two approaches agree within a factor of two 87% of the time; for χ, 78%. These levels of agreement are greater than or comparable to that between the ε and χ values derived from two shear probes and two fast thermistors, respectively, on the same profiler.

1 Introduction

Measurements of oceanic turbulence have been made since the 1950s using platforms and sensors of various shapes and sizes (Lueck et al. 2002). Complete resolution of the turbulence requires measuring temperature and velocity gradients at millimeter-to-centimeter scale. Hence, sampling turbulence is data intensive. Whereas conventional profiling measurements of temperature, conductivity, and pressure are typically sampled at 1 Hz (e.g., Argo floats; Roemmich et al. 2019a), a turbulence profile involves sampling multiple sensors at 100–1000 Hz. A relatively minimal requirement of five separate signals sampled at 100 Hz and recorded at 16-bit resolution equates to 1 kB s^{-1}, or 500 kB per 100 m of profiling range at 0.2 m s^{-1} profiling speed. For floats, this is not a trivial volume of data. For example, transmitting only 3 kB of data from a Deep SOLO float takes 100–200 s (Roemmich et al. 2019b). Extended surfacings also present a danger from surface vessels and vandals. Ultimately, raw turbulence profiles are two-to-three orders of magnitude too large to transmit in a reasonable amount of time.

One approach to reducing turbulence data is given by Rainville et al. (2017) who use it for multi-month glider missions. Onboard the glider, they calculate spectra of raw voltage signals reported by the shear probes and fast thermistors and then band average each of these spectra into 12 bins. After transmission, these binned values are calibrated and fit to model spectra. ~~Although we will share this strategy of postponing calibration ,~~ In other words, they (i) postpone calibration and (ii) minimize the data manipulation and processing that happens onboard. These two strategies are shared by our scheme (and also shared by the reduction scheme developed for χpods; Becherer and Moum 2017). Otherwise, however, our scheme differs from ~~Rainville et al. (2017)~~that of Rainville et al. (2017) as it does not suit our scientific goals of measuring turbulence over the upper $\sim$120 m at high vertical resolution (e.g., $\sim$1 m) and as frequently as possible (see Sect. 2). Two shear probes and two fast thermistors would produce $(2+2)\times 12 = 48$ spectral values per segment. Even without considering the other profiling quantities, the spectral values could add up to $>$20 kB per dive for our scenario. We would be spending as much time transmitting the data as actually measuring the ocean. ~~Instead, we more closely follow Becherer and Moum (2017) who designed a scheme to reduce moored χpod data by more than four orders of magnitude. Overall, our goal is to minimize the file size to be transmitted, and yet also minimize the amount by which we manipulate and process the data onboard.~~

~~Becherer and Moum (2017) showed that , for a given segment, turbulence quantities can be reconstituted from voltage quantities (means, variances, and power law fits). We adapt their approach so that it works for a vertical profiler (~~Our scheme is for profiling instruments that contain shear probes and, optionally, fast thermistors (Sect. 2). First, we document the necessary calibration details (Sect. 3). Next, we compress raw shear voltages by way of simple power law fits and show how ε is derived from these fits in post-processing (Sect. 4). A test of the scheme employing 650 profiles demonstrates that little accuracy is sacrificed in return for a large reduction in data volume (Sect. 5). ~~A similar method and test is given for~~ Knowing ε from the shear probe measurements makes possible a similar method for deriving χ from fast thermistor measurements (Sect. 6 and 7). Adapting the scheme to a different profiler requires minimal modification (Sect. 8). For our ~~particular profiler~~setup, the scheme reduces the dataset size by a factor of ~~240: only 3~~300: only 2.5 kB for each 100 m of a profile (Sect. 9).

2 The Flippin' χSOLO (FCS)

We intend our data reduction scheme to be sufficiently general to be portable to all vertical turbulence profilers that contain shear probes. It can also be used with gliders if a measure of flow speed past the sensors is available (e.g., Greenan et al. 2001; Merckelbach and Carpenter 2021). In a general sense, some of the values specified herein ought to be considered variables (Sect. 8). However, we do have a particular platform for which we are developing the scheme: the Flippin' χSOLO (FCS), and the values used here are chosen for the objective of detailed upper ocean profiling.

FCS is a ~~conventional~~ descendant of the SOLO-II profiling float (Roemmich et al. 2004) with the addition of a turbulence package ~~plus~~ and extra functionality. The turbulence package includes two shear probes (Osborn 1974) to measure small-scale velocity gradients from which ε is computed, two fast thermistors to measure small-scale temperature fluctuations from which χ is computed, ~~as well as a pitot tube (Moum 2015), pressure sensor ,~~ and a pressure sensor from which profiling speed is derived. FCS also includes a three-axis ~~accelerometer, and compass. The pressure sensor yields a measure of profiling speed used in our scheme. The pitot tube, accelerometer, and compass data~~ accelerometer that is used to measure the surface wave field (although with a method not described in this paper). Accelerometer data from when FCS is profiling are not used in ~~the turbulence data reduction schemebut have other purposes~~

such as measuring the surface wave field. When changing its buoyancy to switch our reduction scheme. FCS and its measurements are described more completely in companion paper (Moum et al. under review) .

To reverse profiling direction, FCS also flips (adjusts buoyancy and flips via internal shifting of the battery pack) so that . This causes the turbulence sensors to always point into undisturbed fluid. Flipping therefore permits profiling on both ascent and descent descent and ascent including sampling of the upper 5 m on the upward profile. FCS and its measurements will be described more completely in a future paper. ascent.

As a prototype, a SOLO float without flipping capability but standard (non-flipping) SOLO float with a modified χpod (Moum and Nash 2009) attached was deployed in the Bay of Bengal to measure the suppression of turbulence by salinity stratification (Shroyer et al. 2016). Two This instrument—named χSOLO—did not have shear probes, and therefore could not have provided estimates of ε within mixed layers. (Values of ε can be approximated from χ, but only if there is stratification.) Nevertheless, χSOLO's success motivated the development of the FCS units with flipping capabilities and fully integrated turbulence packages were subsequently built and . These new instruments retained the χ or C in their name despite their ability to also directly measure ε from shear probes.

Two FCS units were vetted over four days in May 2019 off the Oregon coast. During this period, each unit profiled from the surface to $\sim$120 m and back at a typical speed of 0.2 m s^{-1}. Adding time at the surface, each dive cycle took $\sim$30 minutes and we obtained 650 profiles in total.

In this 2019 experiment, one of the shear probes on one of the two units malfunctioned. Hence, the dataset for this paper contains approximately 25% fewer shear data than fast thermistor data.

3 Conversion of measured voltages to physical units

The core of our data reduction scheme uses power law fits of voltage spectra that are calculated onboard, and subsequently converted to meaningful turbulence quantities in post-processing. Additional voltage quantities are also recorded to determine temperature, pressure, and profiling speed.

3.1 Nomenclature and conventions

- All quantities measured by FCS that are discussed in this paper are sampled at 100 Hz.
- All voltage spectra are frequency spectra and denoted $\Psi_x(f)$ (where x is a label such as s for shear) with units of $V^2\,Hz^{-1}$.
- Physical spectra of shear and temperature gradient are wavenumber spectra and denoted $\Phi_x(k)$ with units of $s^{-2}\,cpm^{-1}$ and $K^2\,m^{-2}\,cpm^{-1}$, respectively. Figure 4 is an exception in which shear spectra are frequency spectra: $\Phi_s(f)$.
- Wavenumber k has the unit cycles per meter (cpm). Expressions quoted from other papers may differ by factors of 2π for wavenumbers in radians per meter.
- The Kraichnan model spectrum Φ_{Kr} primarily depends on the dissipation rates of turbulent kinetic energy and temperature variance (ε and χ), but it also depends on the molecular viscosity ν and molecular thermal diffusivity D_T. For brevity, we write $\Phi_{Kr}(k,\varepsilon,\chi)$ rather than the more complete $\Phi_{Kr}(k,\varepsilon,\chi,\nu,D_T)$. Similarly, the Nasmyth spectrum is written $\Phi_{Na}(k,\varepsilon)$ rather than $\Phi_{Na}(k,\varepsilon,\nu)$. In cases where the arguments are unambiguous or unimportant, we simply write Φ_{Na} and Φ_{Kr}.
- A pair of angle brackets, $\langle\cdot\rangle$, denotes the mean value over a segment of length $N_{seg} = 512$ data points. This equates to $\sim$1 m at our nominal profiling speed of $0.2\,m\,s^{-1}$.
- To calculate spectra for a given 512-element voltage segment, we first remove the linear trend, then use three half-overlapping, Hamming-windowed, 256-element subsegments (i.e., $N_{fft} = 256, N_{overlap} = 128$).

In general, the values of N_{seg} and N_{fft} are variables. Our choices are based on the 100 Hz sampling ($\sim$500 cpm) and the goals of FCS, which include obtaining high-vertical-resolution turbulence data, especially near the surface. For different turbulence profilers or different scientific goals, longer segments and/or more overlapping subsegments may be more appropriate (see Sect. 8).

We do not pursue the possibility of using accelerometers to decontaminate spectra (e.g., Levine and Lueck 1999) ; three subsegments is too few for this to work well. Rather, we focus on a frequency band that we know to be unaffected by vibration.

3.2 Shear calibration

The voltage reported by the shear probe V_s is linearly proportional to shear:

$$u_z = \frac{\alpha}{W^2} V_s \tag{1}$$

$$\alpha = 1/(2\sqrt{2}\rho G_s T_s S_s) \tag{2}$$

where W is the flow speed past the sensor. The overall engineering calibration α includes the seawater density ρ, the analog circuit gain G_s (equal to 1 for FCS circuitry), the probe sensitivity S_s ($\sim 0.25 \times 10^{-3}$ V m^2 N^{-1}) and the differentiator time constant T_s ($\sim$1 s).

The linearity in V_s admits a simple link between the physical and voltage spectra:

$$\Phi_{u_z}(k) = \frac{1}{H_s^2(k)} \frac{\alpha^2}{W^3} \Psi_s(f). \tag{3}$$

where $H_s^2(k)$ is the transfer function that accounts for (i) spatial averaging by the shear probe of high-wavenumber motions and (ii) analog and digital filtering of the raw voltage signal (see Appendix A). Note also the use above of the following relation:

$$\Psi(f) = \Psi(k) \frac{\mathrm{d}k}{\mathrm{d}f} = \frac{\Psi(k)}{W}. \tag{4}$$

3.3 Temperature and temperature gradient calibration

Two voltage signals are recorded for each fast thermistor. V_T is the voltage output directly related to T and V_{Tt} is the differentiated output, which improves resolution at high frequencies ($\gtrsim$10 Hz). Temperature is related to V_T through a quadratic calibration:

$$T = C_{1T} + C_{2T} V_T + C_{3T} V_T^2 \tag{5}$$

$$\langle T \rangle = C_{1T} + C_{2T} \langle V_T \rangle + C_{3T} \left\langle V_T^2 \right\rangle \tag{6}$$

where C_{1T}, C_{2T}, and C_{3T} are coefficients determined from lab calibrations. ~~Note how $\langle T \rangle$ depends on the means of both V_T and V_T^2 because of the quadratic calibration~~Eq. (6) is technically an approximation because it contains $\langle V_T \rangle^2$, not $\langle V_T^2 \rangle$, but over 5 s time scales this changes $\langle T \rangle$ by $\lesssim$0.001°C (estimated from the 2019 dataset).

The gradient of ~~this~~ the temperature calibration is

$$\frac{\partial T}{\partial V_T} = C_{2T} + 2C_{3T}V_T \approx C_{2T} + 2C_{3T}\langle V_T \rangle . \tag{7}$$

~~Over 5 s time scales, we consider V_T to be constant.~~ Consequently, the small-scale vertical temperature gradient T_z is linearly proportional to the differentiated voltage V_{Tt}. To demonstrate, we first rewrite T_z in terms of more directly measured quantities:

$$T_z = \frac{\partial T}{\partial z} = \frac{\partial T}{\partial V_T}\frac{\partial V_T}{\partial t}\frac{\partial t}{\partial z}. \tag{8}$$

The first quantity on the right-hand side is Eq. (7), the last is $1/W$, and the second is

$$\frac{\partial V_T}{\partial t} = \frac{V_{Tt}}{C_{Tt}} \tag{9}$$

where C_{Tt} is the gain of the analog differentiator.

Rewriting Eq. (8), the aforementioned linear relationship between T_z and V_{Tt} becomes

$$T_z = \left(\frac{C_{2T} + 2C_{3T}\langle V_T \rangle}{C_{Tt}W}\right) V_{Tt}. \tag{10}$$

The relationship between physical and voltage spectra is therefore

$$\Phi_{T_z}(k) = \frac{1}{H^2_{Tt}(k)}\left(\frac{C_{2T} + 2C_{3T}\langle V_T \rangle}{C_{Tt}}\right)^2 \frac{1}{W}\Psi_{Tt}(f). \tag{11}$$

Again, we have invoked Eq. (4) and the transfer function $H^2_{Tt}(k)$ is defined in Appendix A.

3.4 Pressure and profiling velocity calibration

Pressure has a linear calibration:

$$P\,[\mathrm{dbar}] = \frac{C_{1P} + C_{2P}V_P}{1.45\,\mathrm{psi\,dbar^{-1}}} - p_{\mathrm{atm}}. \tag{12}$$

In our usage, the coefficients C_{1P} and C_{2P} are recorded in units of psi and $\mathrm{psi\,V^{-1}}$, respectively, and calibrated under total pressure. Subtracting atmospheric pressure makes $P = 0$ at the sea surface. The constant C_{1P} must account for the vertical position of the pressure sensor on the instrument relative to

the shear probes and thermistors. Hence, C_{1P} differs between upcasts and downcasts. For the reduced dataset, we ~~want $\langle P \rangle$, which is simply Eq. (12) with $\langle V_P \rangle$ in place~~ record the last pressure voltage in each segment. For example, with $N_{\text{seg}} = 512$, we save the 512th, 1024th, and 1536th values of V_P ~~.~~ for the first three segments. The average pressure in the second and third segment are $0.5(V_P(1024) + V_P(512))$ and $0.5(V_P(1536) + V_P(1024))$, respectively. The average pressure in the first segment is found by extrapolation.

The flow speed past the sensors, denoted W, is derived from the ~~pressure voltage~~ rate of change ~~. Over a segment of length N, the mean of W is a scaled version of the difference between the first and Nth voltage values~~of the pressure voltages just described:

$$\langle W \rangle = \frac{\partial P}{\partial t} = \frac{C_{2P}}{1.45} \underbrace{\frac{|\Delta V_P|}{N_{\text{seg}} \Delta t}}_{\text{Calculate onboard}} \tag{13}$$

where Δt is the sampling period (here 0.01 s) ~~, and ΔV_P is $V_P(N) - V_P(1)$.~~ and ΔP is $V_P(1024) - V_P(512)$ and $V_P(1536) - V_P(1024)$ for the second and third segments, respectively. Extrapolation is again used for the first segment.

No smoothing is necessary before calculating ΔV_P because its magnitude is so much larger than the quantization of the signal (this being the limiting factor for precision of pressure recorded by FCS). In physical units, P is precise to 0.003 dbar, which is $\mathcal{O}(300)$ times smaller than ΔP.

Wave orbitals can introduce variability when W is small ($\lesssim 0.15\,\mathrm{m\,s^{-1}}$). As a diagnostic we calculate and record the minimum value of W for each segment. This also helps to identify the beginning and end of profiles as shown in Appendix B. In standard processing, we would derive $W(t)$ from the pressure signal low passed at 2 Hz. To avoid the need to low-pass filter the signal onboard, we instead make 10 estimates of $W(t)$ per segment and take the minimum of these:

$$W_{\text{min}} = \frac{C_{2P}}{1.45} \underbrace{\min\left(\frac{|\Delta V_P(t_i)|}{50 \Delta t} \right)}_{\text{Calculate onboard}} \tag{14}$$

where $t_i = 1, 51, 101, \ldots, 501$. Even with this sampling of every 50th element, which follows from sub-sampling a 100 Hz signal at 2 Hz, $\Delta V_P(t_i)$ is large enough that smoothing is unnecessary.

In this paper, we immediately discard all segments in which $W_{\text{min}} < 0.05\,\mathrm{m\,s^{-1}}$. This threshold is reached only at the top and bottom of profiles, if at all. Note, however, that this does not imply that a

segment with $W_{\min} > 0.05\,\mathrm{m\,s^{-1}}$ is trustworthy. Even segments with $W_{\min}$ closer to $0.15\,\mathrm{m\,s^{-1}}$ should be treated with particular caution. Signs that a segment is questionable are that $\langle W \rangle$ and $W_{\min}$ differ by ~~more than~~ ~20% or more and that spectral fit scores are low (see Sect. 4.3 and 6.3). These two issues often co-occur because of the nonlinear relationship between shear and profiling speed (Eq. 1). Low frequency variations in W ultimately lead to spectra that are redder than expected, and hence have low fit scores. Such segments should be discarded. There is not a simple way to correct the spectra given the nonlinearity.

4 Reduction of shear data

In this section, we are ultimately going to fit measured spectra to an inertial subrange model that does not necessarily apply at the relevant frequencies or wavenumbers. We will elaborate as we go, but we want to emphasize in advance that measured spectra do not need to conform to an inertial subrange model for us to obtain accurate values of ε. The inertial subrange is merely a convenient starting point.

4.1 Summarizing Nasmyth spectra with $f^{1/3}$ fits

Shear measurements ideally capture both the inertial and viscous subranges and hence use a wide band of the measured spectrum to derive values for ε. In practice, noise and sensor resolution limit how well the true environmental spectrum is resolved. Conventional work-arounds exploit the Nasmyth model spectrum $\Phi_{\mathrm{Na}}(k,\varepsilon)$ (Nasmyth 1970; Oakey 1982). One approach is to iterate toward a solution in which the integral of Φ_{Na} over a specific wavenumber band matches that of the measured spectrum Φ_{u_z} (e.g., Moum et al. 1995). Another is to find the best fit of Φ_{u_z} to Φ_{Na} by using maximum likelihood estimation together with a model of the expected statistical distribution of the spectral coefficients being fitted (e.g., Bluteau et al. 2016).

Here we develop a new and simpler two-stage approach to fitting shear spectra to Φ_{Na}. In the first stage, we use an $f^{1/3}$ power law fit over a fixed frequency range of f_{l} to $f_{\mathrm{h}} = 1$–$5\,\mathrm{Hz}$, where $f^{1/3}$ follows from the assumption that we are fitting over the inertial subrange. In ~~this~~ the second stage, we correct for when this often-invalid assumption.

In the inertial subrange, shear spectra are proportional to $k^{1/3}$ and hence also $f^{1/3}$ since $f = Wk$. With $N_{\mathrm{fft}} = 256$ and 100 Hz sampling (Sect. 3.1), spectral coefficients are separated by frequency increments of

100 Hz/256 = 0.39 Hz, so there are 10 coefficients between 1 and 5 Hz. (Our processing code will actually use bounding frequencies of 0.98 and 4.88 Hz as these are half-integer multiples of 0.39 Hz, but for brevity we will write these as 1 and 5 Hz throughout.)

Our choice of $f_l = 1$ Hz is dictated by a requirement that we avoid low frequency contamination induced by (i) advection by wave orbital motion and (ii) pitch and roll motions of the profiler. Together, these dominate below 0.3 Hz. Setting $f_l = 0.5$ Hz would add only one more spectral coefficient. Our choice of $f_h = 5$ Hz is a trade-off between maximizing the bandwidth of the fit and minimizing how much measured spectra are subject to either noise or viscous roll off. Other profilers may benefit from different frequency bounds (see Sect. 8).

Our inertial subrange assumption is often false. Indeed, 'assumption' is perhaps a misnomer as we do not expect it to be true; we know that viscous roll off will often occur at frequencies lower than 5 Hz (25 cpm for a nominal value of $W = 0.2\,\mathrm{m\,s^{-1}}$). However, because there exists an analytical expression for the viscous roll off, we are able to derive an exact expression that quantifies how much ε is underestimated. This is the second stage of our approach. We derive an expression for the correction function F_{Na} in such a way that it can be calculated in post-processing. The benefits of this approach are that (i) we can fit uncalibrated (i.e., voltage) spectra and (ii) it simplifies the actual onboard fitting routine (Sect. 4.2).

The full Nasmyth spectra and its inertial range approximation are as follows (Lueck 2013):

$$\Phi_{\mathrm{Na}}(k,\varepsilon) = \frac{\varepsilon^{3/4}}{\nu^{1/4}} \frac{8.05(k\eta)^{1/3}}{1+(20.6k\eta)^{3.715}} \tag{15}$$

$$\Phi_{\mathrm{Na}}(k \lesssim 0.02/\eta, \varepsilon) = 8.05 k^{1/3} \varepsilon^{2/3} \tag{16}$$

where $\eta = (\nu^3/\varepsilon)^{1/4}$ is the Kolmogorov length scale.

~~Consider an $f^{1/3}$ fit of the Nasmyth spectrum over~~ Let $\varepsilon_{\mathrm{init}}$ denote the *initial* value of ε that comes from fitting a measured spectrum to the approximate form in Eq. (16) using the simple power-law fitting method in Appendix C, rather than fitting to the full form in Eq. (15). As noted earlier, the fit will be over the f_l–f_h = 1–5 Hz ~~for two values of ε: 1×10^{-9} and $1\times10^{-6}\,\mathrm{W\,kg^{-1}}$ (Fig. 1a). With~~ range which, given our nominal value of $W = 0.2\,\mathrm{m\,s^{-1}}$, ~~we get~~ equates to k_l–k_h = 5–25 cpm. ~~For~~

Consider two contrasting examples of low and high turbulence with $\varepsilon = 1\times10^{-9}$ and $1\times10^{-6}\,\mathrm{W\,kg^{-1}}$, respectively. For now, assume the measured spectrum to be fit is itself a Nasmyth spectrum. For $\varepsilon = 10^{-6}\,\mathrm{W\,kg^{-1}}$ the $f^{1/3}$ fit lies on top of Φ_{Na}. Conversely, the $f^{1/3}$ fit for the smaller ε value is seemingly

meaningless: the $f^{1/3}$ fit (dashed line) does not even match the sign of the slope of Φ_{Na}. Worse yet, naively inverting this ~~*initial* (or 'init')~~ initial fit produces the underestimate $\varepsilon_{\mathrm{init}} = 1.2 \times 10^{-10}\,\mathrm{W\,kg^{-1}}$, ~~six~~ eight times smaller than the true value of ε. However, by adjusting by a factor of $1/F_{\mathrm{Na}}$, defined in the following paragraph, the fit (dotted line) ~~now~~ looks like a hypothetical extrapolation of the inertial subrange. Equivalently, $\varepsilon_{\mathrm{init}}$ is corrected to the true value of ε as

$$\varepsilon = \varepsilon_{\mathrm{init}} / F_{\mathrm{Na}}^{3/2}. \tag{17}$$

In our example, $1 \times 10^{-9}\,\mathrm{W\,kg^{-1}} = 1.2 \times 10^{-10}\,\mathrm{W\,kg^{-1}} / 0.238^{3/2}$. The value of 0.238 is the solution to an implicit equation derived below that depends on $\varepsilon_{\mathrm{init}}$ and W. For clarity, our demonstration starts by assuming we know ε rather than $\varepsilon_{\mathrm{init}}$.

Nasmyth spectra can be flattened to unity over the inertial subrange with the normalization $8.05k^{1/3}\varepsilon^{2/3}$ (Fig. 1b). Values of F_{Na} are based on the mean of these flattened spectra over the wavenumber range k_{l}–k_{h} ($= f_{\mathrm{l}}/W$–f_{h}/W):

$$F_{\mathrm{Na}} = \frac{1}{k_{\mathrm{h}} - k_{\mathrm{l}}} \int_{k_{\mathrm{l}}}^{k_{\mathrm{h}}} \frac{\Phi_{\mathrm{Na}}(k,\varepsilon)}{8.05k^{1/3}\varepsilon^{2/3}} \mathrm{d}k. \tag{18}$$

To remove the dependence of the true value of ε, we substitute ~~using Eq. (17) . Further, to account for the $H_s^2(k)$ factor in Eq. (3), we make the substitution~~

$\Phi_{\mathrm{Na}}(k,\varepsilon) \rightarrow H_s^2(k)\,\Phi_{\mathrm{Na}}(k,\varepsilon).$

~~Think of this substitution as inverting the conventional way that $H_s^2(k)$ is invoked. Usually, a measured shear spectrum is amplified at high wavenumbers by $1/H_s^2(k)$ and then fit to the model spectrum Φ_{Na}. Here, instead of amplifying the measured spectrum, we reduce the model spectrum. With this latter approach, $H_s^2(k)$ is calculated and applied only during the post-processing stage. (It changes F_{Na} by only ~5% since we fit over relatively low wavenumbers.) Altogether, the substitutions result in~~ Eq. (17) to produce an implicit function for F_{Na}, which can be solved numerically:

$$\frac{1}{k_{\mathrm{h}} - k_{\mathrm{l}}} \int_{k_{\mathrm{l}}}^{k_{\mathrm{h}}} \frac{H_s^2(k)\,\Phi_{\mathrm{Na}}(k, \varepsilon_{\mathrm{init}}/F_{\mathrm{Na}}^{3/2})}{8.05k^{1/3}\varepsilon_{\mathrm{init}}^{2/3}/F_{\mathrm{Na}}} \frac{\Phi_{\mathrm{Na}}(k, \varepsilon_{\mathrm{init}}/F_{\mathrm{Na}}^{3/2})}{8.05k^{1/3}\varepsilon_{\mathrm{init}}^{2/3}/F_{\mathrm{Na}}} \mathrm{d}k - F_{\mathrm{Na}} = 0. \tag{19}$$

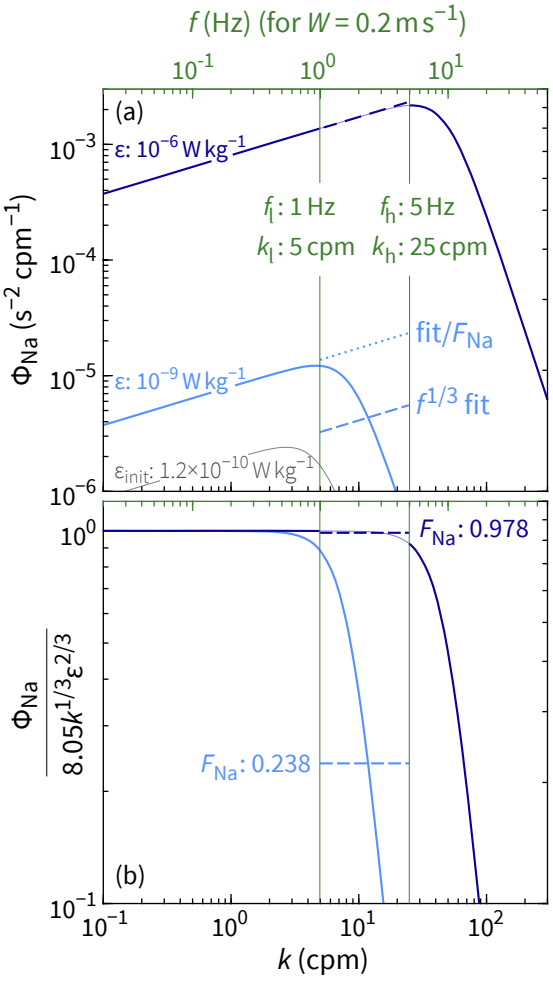

Figure 1. Calculation of the correction function F_{Na} for two values of ε. For $\varepsilon = 1 \times 10^{-6}\,\mathrm{W\,kg^{-1}}$, a $k^{+1/3}$ power law is a good approximation of the Nasmyth spectrum over the frequency range f_{l}–f_{h} (1–5 Hz) for a profiling speed of $W = 0.2\,\mathrm{m\,s^{-1}}$. Although the same is not true for $\varepsilon = 1 \times 10^{-9}\,\mathrm{W\,kg^{-1}}$, we can account for the roll off with a factor of F_{Na}. F_{Na} can be defined in terms of either ε (Eq. (18)) or $\varepsilon_{\mathrm{init}}$ (Eq. (19)). Panel b takes the former approach. In practice, we must take the latter approach since we do not know ε until after it is derived from $\varepsilon_{\mathrm{init}}$ and F_{Na}.

Note how the two forms of F_{Na} (Eqs. 18 and 19) are defined with different arguments. For our example, $F_{\mathrm{Na}}(\varepsilon = 1 \times 10^{-9}\,\mathrm{W\,kg^{-1}}) = F_{\mathrm{Na}}(\varepsilon_{\mathrm{init}} = 1.2 \times 10^{-10}\,\mathrm{W\,kg^{-1}}) = 0.238$. Hereafter, we use the latter: $F_{\mathrm{Na}}(\varepsilon_{\mathrm{init}})$.

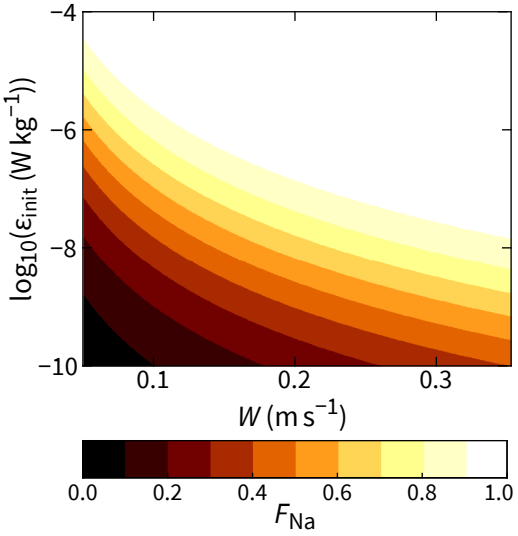

Figure 2. The correction function $F_{\rm Na}$ for $\nu = 1 \times 10^{-6}\ {\rm m^2\ s^{-1}}$ and $f_{\rm l}$–$f_{\rm h}$ = 1–5 Hz.

With $f_{\rm l}$ and $f_{\rm h}$ fixed, $F_{\rm Na}$ is a function of three variables: $\varepsilon_{\rm init}$, W, and ν. $F_{\rm Na}$ is closer to one (less of a correction) for larger values of $\varepsilon_{\rm init}$ (Fig. 1). It is also closer to one for higher values of W (Fig. 2) since $k_{\rm l}$ and $k_{\rm h}$ decrease with increasing W (i.e., $k_{\rm l}$–$k_{\rm h}$ moves closer to the inertial subrange).

To simplify calculations in the upcoming section, we make one final change to Eq. (19) using the substitution

$$\Phi_{\rm Na}(k,\varepsilon) \rightarrow H_s^2(k)\,\Phi_{\rm Na}(k,\varepsilon). \tag{20}$$

Therefore,

$$\frac{1}{k_{\rm h}-k_{\rm l}}\int_{k_{\rm l}}^{k_{\rm h}} \frac{H_s^2(k)\,\Phi_{\rm Na}(k,\varepsilon_{\rm init}/F_{\rm Na}^{3/2})}{8.05k^{1/3}\varepsilon_{\rm init}^{2/3}/F_{\rm Na}}{\rm d}k - F_{\rm Na} = 0. \tag{21}$$

Think of this substitution in Eq. (20) as inverting the conventional way that $H_s^2(k)$ is invoked. Usually, a measured shear spectrum is amplified at high wavenumbers by $1/H_s^2(k)$ and then fit to the model spectrum $\Phi_{\rm Na}$. Here, instead of amplifying the measured spectrum, we reduce the model spectrum. With this latter approach, $H_s^2(k)$ is calculated and applied only during the post-processing stage. (It changes $F_{\rm Na}$ by only ~5% since we fit over relatively low wavenumbers.)

4.2 Obtaining $\varepsilon_{\text{init}}$ from shear voltage spectra

Since ε can be reconstructed from $\varepsilon_{\text{init}}$, we require an expression linking $\varepsilon_{\text{init}}$ to the shear voltage spectrum Ψ_s. Equating Eq. (3) and Eq. (16) gives

$$\frac{\alpha^2}{W^3}\Psi_s(f) = 8.05k^{1/3}\varepsilon_{\text{init}}^{2/3} \tag{22}$$

where we have left out $H_s^2(k)$ since it has been incorporated into F_{Na}. Rearranging and substituting $k = f/W$ gives

$$\varepsilon_{\text{init}}^{2/3} f^{1/3} = \frac{\alpha^2}{8.05W^{8/3}}\Psi_s(f). \tag{23}$$

Then, to solve for $\varepsilon_{\text{init}}$, we use a least-squares fit (see Appendix C):

$$\varepsilon_{\text{init}}^{2/3} = \frac{\alpha^2}{8.05W^{8/3}} \underbrace{\frac{\sum_f f^{1/3}\Psi_s}{\sum_f f^{2/3}}}_{\text{Calculate onboard}} \tag{24}$$

where the sums are understood to be over the range f_{l}–f_{h}. The quantities α, W, and $\varepsilon_{\text{init}}$ are calculated in post-processing.

4.3 Quality control of the shear spectral fits

Measured shear spectra are often quality controlled either by manual visual inspection or, more objectively, by quantifying the level of mismatch between them and their associated model. Possible mismatch quantities include the mean absolute deviation or the variance of the ratio $\Phi_{u_z}/\Phi_{\text{Na}}$ (e.g., Ruddick et al. 2000; Bluteau et al. 2016). We cannot calculate such quantities with our reduced scheme because we do not know what each spectrum should look like until we calculate its ε value in the post-processing stage. (Recall that Φ_{Na} is a function of ε.) By this stage, we have lost information about the spectral shape through the summing operation in Eq. (24).

To retain at least some information about the shape of each voltage spectrum, we will split the 1–5 Hz range and compute two fits rather than one. Doing so allows for a first-order check that the spectrum over the 1–5 Hz range approximately follows the expected shape.

Mathematically, there is nothing special about our choice f_{l}–f_{h} = 1–5 Hz. In theory, we can split the 1–5 Hz range into two (1–3 Hz and 3–5 Hz) and obtain a value of $\varepsilon_{\text{init}}$ for each. These values will differ,

but so will the associated values of F_{Na}. For a measured spectrum that conforms to a Nasmyth spectrum, the two values of ε calculated with Eq. (17) will not differ (Fig. 3). We therefore calculate onboard the sums in Eq. (24) over both f_{l}–f_{m} and f_{m}–f_{h}, where the mid frequency $f_{\mathrm{m}} = 3\,\mathrm{Hz}$. (In our code, f_{m} is actually $7.5 \times 0.39\,\mathrm{Hz} = 2.93\,\mathrm{Hz}$ for the reason given in Sect. 4.1.) Hence, for each spectrum we are able to post-process to recover two independent estimates of ε, denoted $\varepsilon_{\mathrm{l–m}}$ and $\varepsilon_{\mathrm{m–h}}$. The mean of these two provides a single, final value for ε, and their ratio quantifies the match of a measured spectrum to a Nasmyth spectrum over the range f_{l}–f_{h}:

$$\varepsilon = \mathrm{mean}\left(\varepsilon_{\mathrm{l–m}}, \varepsilon_{\mathrm{m–h}}\right) \tag{25}$$

$$\varepsilon \text{ fit score} = \frac{\min\left(\varepsilon_{\mathrm{l–m}}, \varepsilon_{\mathrm{m–h}}\right)}{\max\left(\varepsilon_{\mathrm{l–m}}, \varepsilon_{\mathrm{m–h}}\right)}. \tag{26}$$

The best possible fit score is 1; the lower the score, the poorer the fit~~(Fig. 4).~~. The example spectra in Fig. 4 show that a high fit score does not necessarily imply small residuals. Rather, fits with high scores are typically those with random residuals meaning that a given measured spectral coefficient is just as likely to be above the fit as below it. Fits with low fit scores are typically those with autocorrelated residuals meaning that the sign and/or magnitude of a residual is correlated with that of its neighbors. In practice, we expect a range of ε fit scores: instantaneous and unaveraged spectra differ from the Nasmyth spectrum because they are derived from a limited sampling of a statistical process, and ~~they can also deviate~~ because of non-stationarity, anisotropy, and inhomogeneity of the turbulence.

When ε is small ($\lesssim 10^{-9}\,\mathrm{W\,kg^{-1}}$), the fit score may be consistently low if spectral coefficients in the f_{m}–f_{h} range are affected by noise and consequently $\varepsilon_{\mathrm{m–h}} \gg \varepsilon_{\mathrm{l–m}}$. For such cases, we choose to use only the lower-frequency fit. We would rather have a more accurate estimate of ε and forgo the fit score than have a biased-high ε value with a biased-low fit score. (Either way, the small values of ε in question will have minimal effect on any averages given that turbulence ~~is approximately lognormal~~distributions have high kurtosis, so high values dominate means.) Specifically,

$$\left.\begin{array}{rcl} \varepsilon & = & \varepsilon_{\mathrm{l–m}} \\ \varepsilon \text{ fit score} & = & — \end{array}\right\} \text{ if } 0.1W\left(\frac{\varepsilon_{\mathrm{l–m}}}{\nu^3}\right)^{1/4} < f_{\mathrm{m}}, \tag{27}$$

where the threshold is equivalent to $k < 0.1/\eta$ with η the Kolmogorov length scale estimated from $\varepsilon_{\mathrm{l–m}}$. For reference, Φ_{Na} peaks at $k = 0.026/\eta$ and rolls off to 11% of its maximum by $k = 0.1/\eta$ (see Eq. (15)).

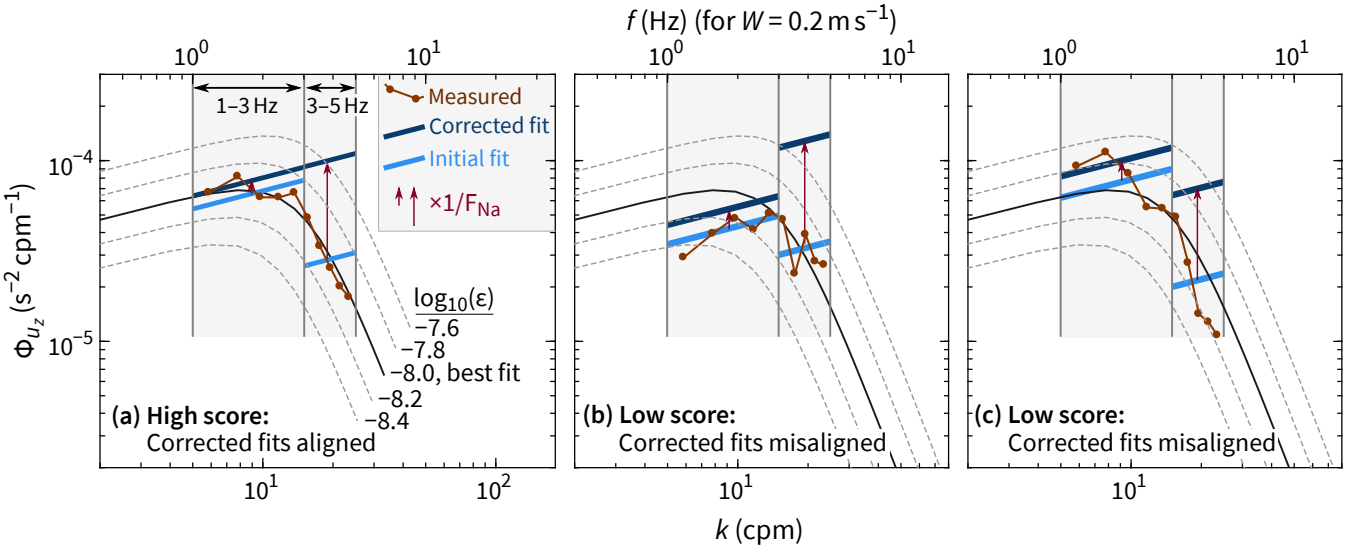

Figure 3. A visual demonstration of how the ε fit score (Eq. (26)) characterizes better and worse fits. For all three ~~examples~~of these hypothetical spectra, ε values from the two fits (1–3 and 3–5 Hz) average to ~~$\varepsilon = 1 \times 10^{-8}$~~$\varepsilon = 1.0 \times 10^{-8}$ W kg^{-1}. Only in panel a, however, does the measured spectrum agree well with the Nasmyth spectrum for this ε value. In practice, the initial fits would be undertaken on voltage spectra~~. Here~~; here, we are using physical units for simplicity. In all three examples, the kinematic viscosity is $\nu = 10^{-6}$ m^2 s^{-1}.

5 Test of the reduction scheme for ε

To test the accuracy of the shear reduction scheme described in the previous section, we apply it retrospectively to the dataset from the 2019 test cruise (Sect. 2). We compare the results to those obtained with the standard processing scheme. This standard scheme (Appendix D) features a more sophisticated despiking routine than used for our reduced scheme, which employs a three standard deviation threshold filter (Appendix E).

A profile-by-profile comparison of the two schemes is shown in Fig. 5. The comparison is then extended to all 650 profiles (>77 000 segments of shear), where we find that ε from the reduced scheme ($\varepsilon_{\text{init}}/F_{\text{Na}}^{3/2}$) is within a factor of two of that from the standard scheme 87% of the time over the full range of measured values, $10^{-10} < \varepsilon < 10^{-4}$ W kg^{-1} (Fig. 6a–b). For comparison, in only 72% do we obtain a factor-of-two agreement between the two independent values of ε measured on the unit with two working shear probes (not shown). Further, to obtain this 87% agreement, we clearly need the correction function F_{Na}:

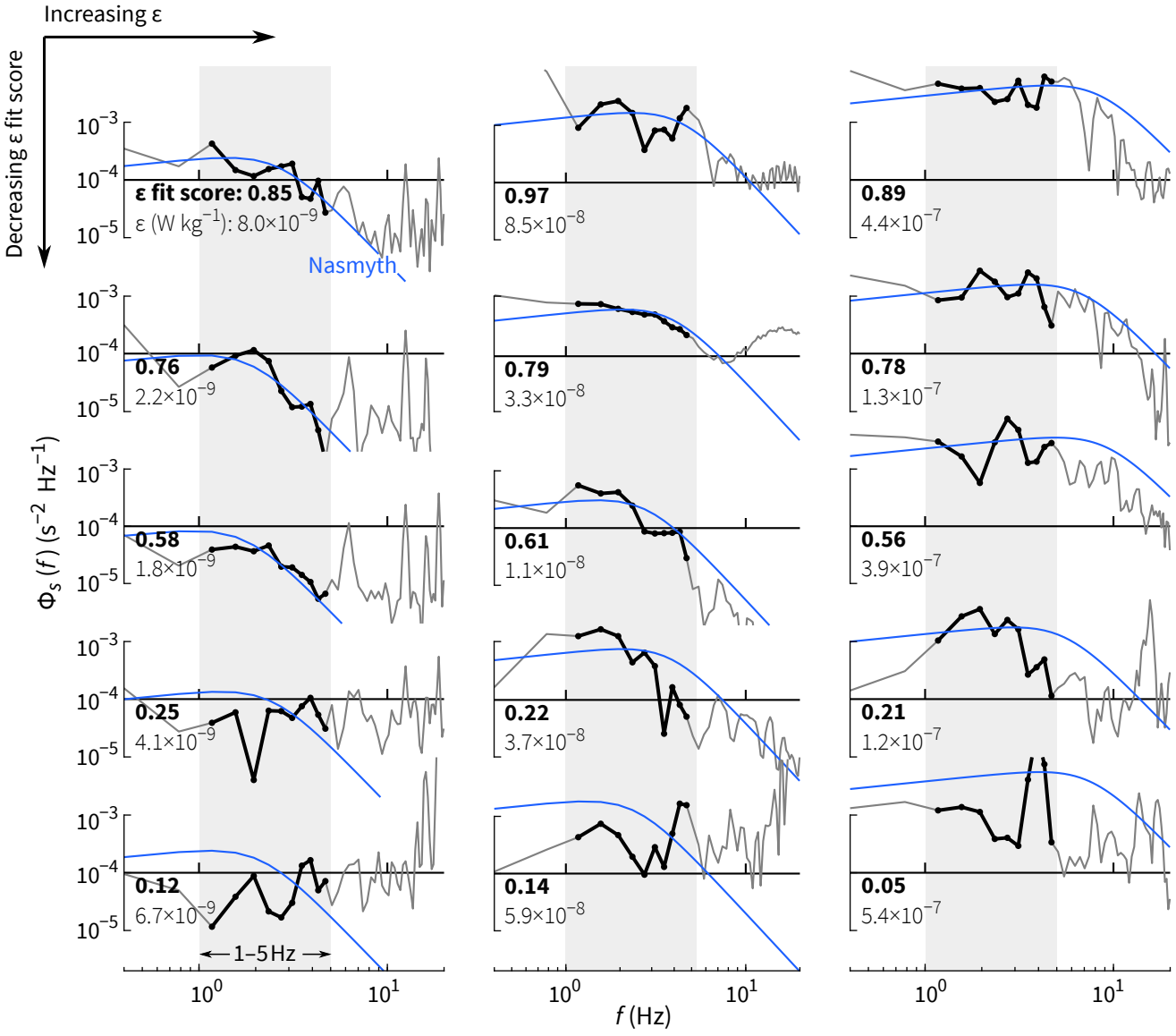

Figure 4. Examples of measured shear spectra exhibiting a range of ε fit scores (Eq. (26)). The best ~~fit is~~ fits are at the top with progressively worse fits (lower scores) moving downward. The examples in each column have (left) $\varepsilon = 10^{-9}$–10^{-8}, (middle) $\varepsilon = 10^{-8}$–10^{-7}, and (right) $\varepsilon = 10^{-7}$–$10^{-6}\,\mathrm{W\,kg^{-1}}$. Each score is only based on spectral coefficients from 1–5 Hz, but lower and higher frequencies are shown for reference.

Fig. 6c shows that the uncorrected values $\varepsilon_{\mathrm{init}}$ only have 1:1 agreement with ε from the standard scheme if $\varepsilon \gtrsim 10^{-7}\,\mathrm{W\,kg^{-1}}$. For the lowest values of ε, the ratio is closer to 1:30.

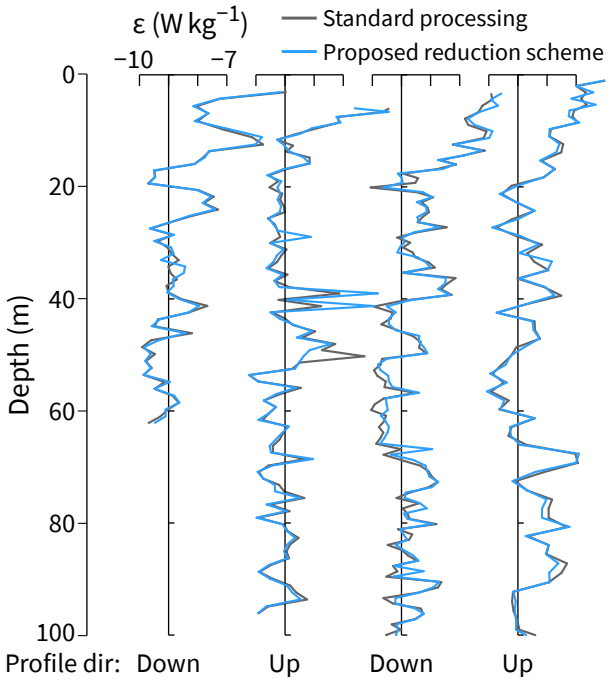

Figure 5. Testing the proposed data reduction scheme for shear measurements against the standard processing approach. One upward and one downward profile from each of the two FCS units were arbitrarily chosen for this comparison.

To demonstrate the ability of the ε fit score to characterize spectra, we show two-dimensional histograms of non-dimensionalized spectral coefficients from all 77 000 measured shear spectra separated into three classes based on their ε fit score: 0.67–1.00, 0.33–0.67, and 0.00–0.33. Only the lowest scoring class fails to collapse to the Nasmyth spectrum (~~Fig. 7c~~Figs 7c, 7f).

6 Reduction of fast thermistor data

The scheme to reduce fast thermistor data to enable measurement of χ is much like the scheme to reduce shear data. As in Sect. 4, we first show how we summarize a model spectrum in terms of a power law fit and a correction factor. (In this case, the correction factor partly depends on the values of ε calculated in Sect. 4.) Then we derive the implementation in terms of voltages and calculate a spectral fit metric.

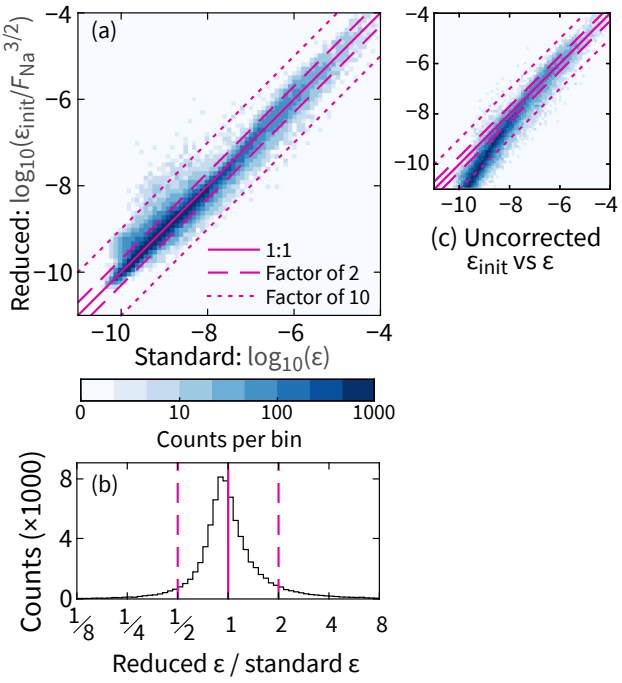

Figure 6. Statistical test of the proposed data reduction scheme for ε based on all 650 profiles (77 000 segments). (a) A comparison that includes the dependence on ε. (b) Further summarized data that exclude this dependence. (c) As for panel a, but uncorrected ($F_{\mathrm{Na}} = 1$).

6.1 Summarizing Kraichnan spectra with f^1 fits

Here we take the Kraichnan spectrum Φ_{Kr} (Kraichnan 1968) as our model and for its low-wavenumber approximation we use the viscous–convective subrange, which scales as k^{+1}. In units of $\mathrm{K}^2\,\mathrm{m}^{-2}\,\mathrm{cpm}^{-1}$, Φ_{Kr} and its approximation are as follows (e.g., Peterson and Fer 2014):

$$\Phi_{\mathrm{Kr}}(k,\varepsilon,\chi) = 4\pi^2 k\chi q\sqrt{\nu/\varepsilon}\,\exp\left(-\sqrt{6q}2\pi k\lambda_B\right) \tag{28}$$

$$\Phi_{\mathrm{Kr}}(k \ll \lambda_B^{-1},\varepsilon,\chi) = 4\pi^2 k\chi q\sqrt{\nu/\varepsilon}. \tag{29}$$

where the Batchelor length scale $\lambda_B = (\nu D_T^2/\varepsilon)^{1/4}$ and q is a constant taken to be 5.26. This expression does not include a $k^{+1/3}$ inertial–convective subrange, which we ignore here as it increases the integral of the temperature gradient spectrum from $k = 0$ to $k = \infty$ by less than 1% and therefore has negligible effect on our results.

A fit against Eq. (29) can be rearranged to give χ_{init}, which is related to χ through the correction function F_{Kr} as

$$\chi = \chi_{\text{init}} / F_{\text{Kr}}. \tag{30}$$

F_{Kr} is not raised to a power like F_{Na} (Eq. (17)). For small values of k, $\Phi_{\text{Kr}} \propto \chi$ whereas $\Phi_{\text{Na}} \propto \varepsilon^{2/3}$.

The derivation of F_{Kr} is equivalent to F_{Na}. We therefore present only the result:

$$\frac{1}{k_{\text{h}} - k_{\text{l}}} \int_{k_{\text{l}}}^{k_{\text{h}}} \frac{H_{Tt}^2(k)\, \Phi_{\text{Kr}}(k, \varepsilon, \chi_{\text{init}}/F_{\text{Kr}})}{4\pi^2 k (\chi_{\text{init}}/F_{\text{Kr}}) q \sqrt{\nu/\varepsilon}} - F_{\text{Kr}} = 0. \tag{31}$$

Note that $F_{\text{Kr}}(\varepsilon, \chi_{\text{init}}, W)$ depends on the underestimate χ_{init}, but the 'true' or 'corrected' value of ε calculated in Sect. 4.

6.2 Obtaining χ_{init} from fast thermistor voltage spectra

Like we did for $\varepsilon_{\text{init}}$ in Sect. 4.2, we derive the expression for χ_{init} in three steps. First, equate the right hand sides of Eqs. 11 and 29 (excluding the transfer function $H_{Tt}^2(k)$, which is incorporated into Eq. (31)):

$$\left(\frac{C_{2T} + 2C_{3T} \langle V_T \rangle}{C_{Tt}} \right)^2 \frac{1}{W} \Psi_{Tt}(f) = 4\pi^2 k \chi q \sqrt{\nu/\varepsilon}. \tag{32}$$

Then, rearrange while substituting $k = f/W$ to get

$$\chi_{\text{init}} f^1 = \frac{1}{4\pi^2 q \sqrt{\nu/\varepsilon}} \left(\frac{C_{2T} + 2C_{3T} \langle V_T \rangle}{C_{Tt}} \right)^2 \Psi_{Tt}. \tag{33}$$

Finally, solve for χ_{init} using a least-squares fit (Appendix C):

$$\chi_{\text{init}} = \frac{1}{4\pi^2 q \sqrt{\nu/\varepsilon}} \left(\frac{C_{2T} + 2C_{3T} \langle V_T \rangle}{C_{Tt}} \right)^2 \underbrace{\frac{\sum_f f \Psi_{Tt}}{\sum_f f^2}}_{\text{Calculate onboard}}. \tag{34}$$

6.3 Quality control of the temperature gradient spectral fits

The approach to quality controlling the fast thermistor data is the same as that for shear (Sect. 4.3). That is, we fit Ψ_{Tt} over f_{l}–f_{m} and f_{m}–f_{h} (1–3 and 3–5 Hz). This ultimately provides two estimates of χ for

each spectrum, which are combined as follows:

$$\chi = \text{mean}\left(\chi_{\text{l–m}}, \chi_{\text{m–h}}\right) \tag{35}$$

$$\chi \text{ fit score} = \frac{\min\left(\chi_{\text{l–m}}, \chi_{\text{m–h}}\right)}{\max\left(\chi_{\text{l–m}}, \chi_{\text{m–h}}\right)}. \tag{36}$$

We do not apply a low χ threshold equivalent to Eq. (27).

7 Test of the reduction scheme for χ

Profiles of χ from the reduced scheme compare well to the standard processing, albeit with a small bias in one direction for low values and in the other direction for high values (Fig. 8). Across all values, the two approaches agree within a factor of two 78% of the time (Fig. 9). By comparison, 82% of segments exhibit a factor-of-two agreement between χ values from the two fast thermistors on the same unit.

Compared to shear spectra, non-dimensionalized temperature gradient spectra have lower fit scores. Especially for the lowest fit scores, the measured temperature gradient spectra tend to be too high at lower frequencies and ~~vice versa (Fig. 10).~~ too high at frequencies near f_{h} (Fig. 10a–c). As frequency increases beyond f_{h}, the effects of noise and thermal response corrections (Appendix A) begin to dominate.

There are three reasons for the poorer fits to temperature gradient spectra compared to that for shear. First, shapes of temperature gradient spectra are often more variable; the best choice for non-dimensional spectral model can be debated (e.g., Sanchez et al. 2011). Second, the temperature gradient fits depend on ε, so uncertainties in ε propagate into the calculation of χ. Third, for our 2019 experiment, the recorded temperature gradient signals were occasionally affected by digitization noise as a consequence of sampling mixed layers. (Shear signals were not affected by digitization noise.)

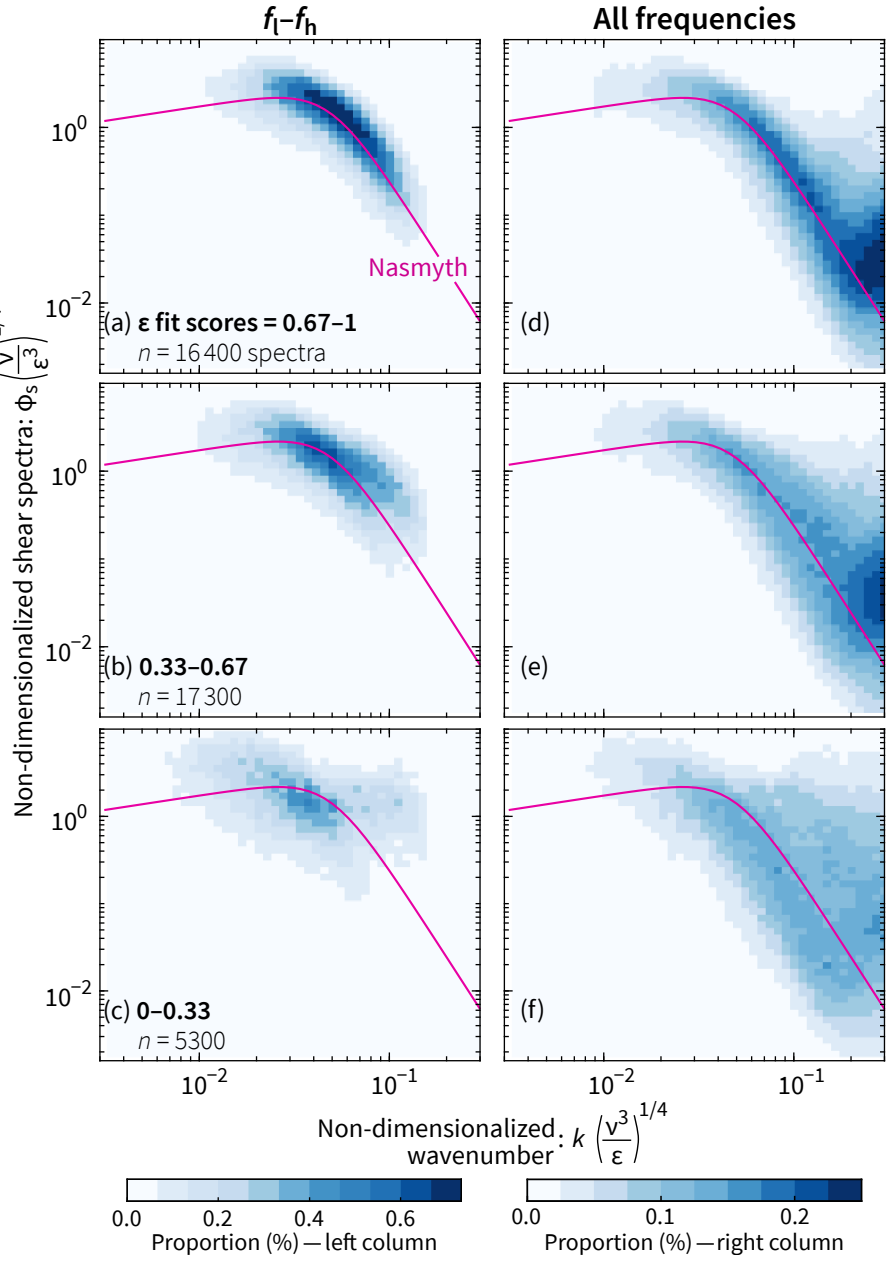

Figure 7. As the ε fit score decreases from top to bottom, there is a corresponding decrease in the level of agreement and tightness of spread between (i) non-dimensionalized, measured shear spectra and (ii) the Nasmyth spectrum. ~~These~~ The two-dimensional histograms in the left column include only spectral coefficients with frequencies between f_l and f_h; those in right column include all frequencies. The total number of spectra in this figure is lower than in Fig. 10 because some low-ε spectra do not have scores (Eq. (27)) and because one of the shear probes failed (Sect. 2).

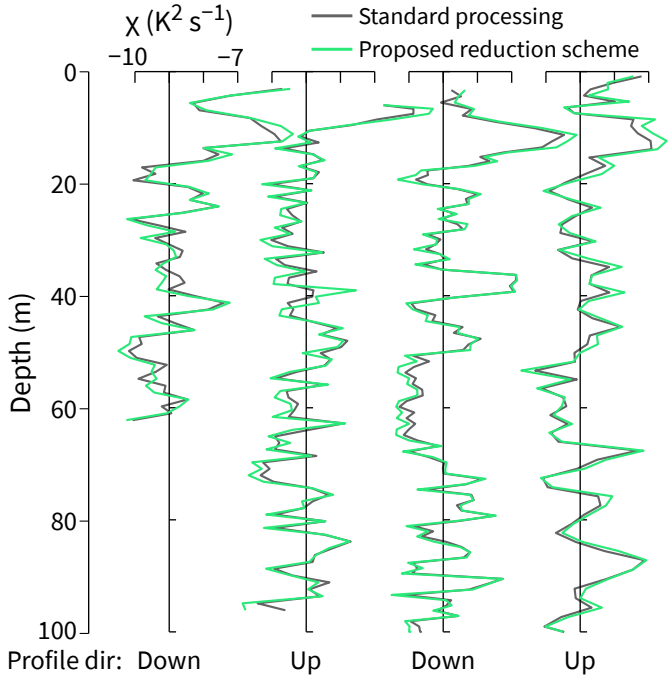

Figure 8. Testing the proposed data reduction scheme for fast thermistor measurements. The profiles used are the same as those chosen in Fig. 5.

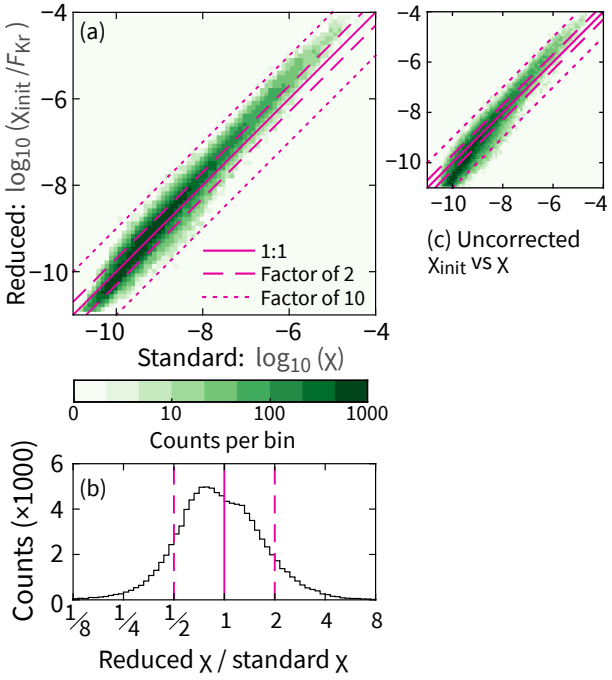

Figure 9. Statistical test of the proposed data reduction scheme for χ. Equivalent to Fig. 6 except for χ not ε. In total, there are 100 000 segments of data.

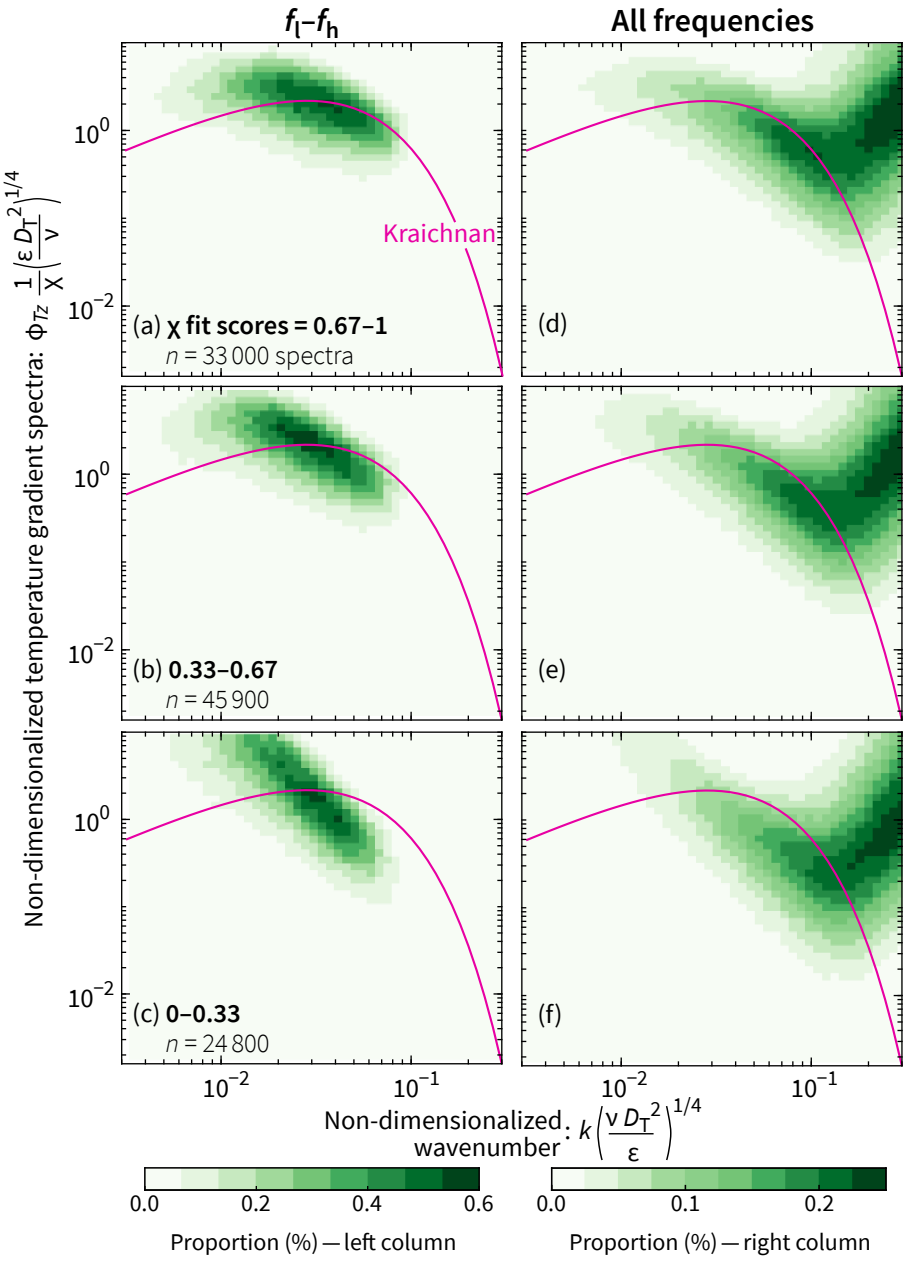

Figure 10. As for Fig. 7, but for temperature gradient rather than shear.

8 Recommendations

8.1 Setting the scheme's parameters

Our scheme requires a few user-defined parameters: f_l, f_h, N_{seg}, and N_{fft}. For this paper, we based these partly on the profiling speed and scientific goals of FCS. For a different profiler, we suggest the following:

- Choose f_h based on a typical profiling speed such that $k_h = f_h/W \approx 25$ cpm for a nominal profiling speed W. For a wide range of ε values, 25 cpm is close to, or beyond, the peak of the Nasmyth spectrum (Fig. 1). ~~Further, ε can be sensitive to the wavenumber fitting range, but centering the fit near $k \approx 10$–20 cpm minimizes this sensitivity (Bluteau et al. 2016).~~ As an example, if FCS profiled at $\sim$0.5 m s^{-1}, we would consider setting $f_h \approx 12$ Hz.

- ~~Keep f_l in the range 0.5–1 Hz. Although our scheme uses the inertial subrange (i.e., low frequencies/wavenumb as its starting point, there is little to be gained by including frequencies of $\mathcal{O}(0.1)$ Hz. A possible exception, albeit tangential to this paper, is if the turbulence measurements come from a platform that effectively measures horizontally. In such cases, FFT segments may be many minutes or more and thereby contain useful low-frequency information (e.g., Bluteau et al. 2011; Moum 2015).~~

- Ensure that there are no known issues such as vibrations that are likely to adversely affect spectral coefficients within the f_l–f_h range. ~~Although vibrational effects can be removed spectrally (Goodman et al. 2006), doing so is beyond the scope of our scheme~~If, however, there are known issues within the desired frequency range, then an alternative approach (one that we did not test) is to use accelerometer signals to correct spectra that are contaminated by vibrations (Levine and Lueck 1999; Goo
.

- Define f_l and f_h separately for shear and temperature gradient if appropriate. Although we set them equal here, this is not necessary.

- Use more than two fitting bands if desired. We use only two bands (1–3 and 3–5 Hz) so as to minimize the file size to be transmitted, but there is nothing preventing there being three or more bands (e.g., adding a 5–7 Hz band). Indeed, this would enable improved estimates of the fit scores (Eqs. 26 and 36) and more flexibility to discard noise-affected bands as in Eq. 27. If file size is less

of an issue such that it is possible to send back fit values for many more than two bands, then the Rainville et al. (2017) scheme outlined in Sect. 1 maybe a better choice than ours.

- Choose N_{seg} and N_{fft} based on scientific goals and, possibly, any logistical constraints; the data reduction scheme is agnostic to these numbers. For example, at the expense of vertical resolution, we could halve the file size of our transmitted dataset by doubling N_{seg} from 512 to 1024.

- Reasonable choices for N_{fft} are $N_{\text{seg}}/2$ or $N_{\text{seg}}/4$, which correspond to three or seven half-overlapping subsegments, respectively. There is little to be gained by diving a segment into even more subsegments so as to produce smoother spectra before fitting. As Ruddick et al. (2000) notes, the task is analogous to fitting a line to 20 points at once or first clumping them in groups of, say, five and then fitting the four averaged points.

8.2 Evaluating the reduced data

One step that cannot be automated is the heuristic evaluation of the reduced turbulence data after they have been converted from voltage quantities to physical ones. For this evaluation, we recommend looking into multiple quantities. First consider the fit scores (Eqs. 26 and 36). ~~These scores work well, but they~~ We recommend discarding any ε or χ values with an associated fit score lower than 0.33. Note, however, that these scores are not a perfect measure of fit. They should be used together with other quality control checks such as comparing

- W and W_{min} (Eqs. 13 and 14) to check whether the profiling speed is constant over a segment;

- ε values from the two shear probes; and

- turbulent features in successive profiles.

The last point is most applicable for a vertical profiler cycling rapidly – for example, twice per hour for FCS. In this case, the profiler is nominally sampling the same vertical fragment of the ocean on a time scale comparable to that over which turbulence evolves. In our experience, many turbulent patches extend over 5–10 profiles.

Recall, also, that all uncertainty in ε propagates into the calculation of χ (Sect. 7). If ε for a given segment cannot be trusted, neither can χ.

9 Conclusions

We have developed a data reduction scheme applicable to vertical profiling of turbulence variables in which each ∼5 s segment is distilled to ~~15~~ 12 quantities (Fig. 11). In post-processing, we reconstruct estimates of ε and χ, associated quality control metrics, and other quantities such as the temperature and profiling speed. The raw data that go into the ~~15~~ 12 quantities are seven different voltages (V_P; V_T and V_{Tt} for each thermistor; and V_s for each shear probe). Hence, for each 512-element segment, we effectively reduce the data by a factor of ~~$512 \times 7/15 \approx 240$~~ $512 \times 7/12 \approx 300$.

This reduction compresses the output data file size for each dive from megabytes to kilobytes. For example, the total amount of data per dive (two profiles) can be estimated assuming our nominal dive depth and profiling velocity of 120 m and 0.2 m s^{-1}. Each dive creates ~~$15 \times 2 \times 120$~~ $12 \times 2 \times 120$ m / (0.2 m s~~$^{-1} \times 5.12$ s) ≈ 3500~~ $^{-1} \times 5.12\,\mathrm{s}) \approx 2800$ quantities. Transmitting each quantity as a 16-bit ~~word~~ float or integer equates to approximately ~~7~~6 kB per dive. This can be reduced by one-third if the spectral fit metrics are suitably scaled logarithmically and then transmitted as 8-bit integers.

One luxury we lose is the ability to inspect the raw signals. Typically this would help to (i) cultivate faith in the data, (ii) flag which segments to discard, and (iii) inform work-arounds such as filtering out potential narrowband vibrations in shear spectra. Our scheme accounts for this constraint in two ways. First, we fit spectra over relatively low frequencies (1–5 Hz) that are unlikely to be affected by noise or vibration. Second, we reduce the data in a way that uses as little arithmetic as possible. Obviously, we cannot reverse-engineer the raw signals, but by making the onboard calculations simple we give ourselves the best chance to later fix or identify any unforeseen issues.

Although the onboard reduction eliminates possibilities in how we process turbulence data, it opens up possibilities in how we obtain turbulence data. By visualizing how turbulence evolves over successive dives in near-real-time, we can concentrate on regions of interest by adapting the dive schedule to profile more frequently or to different depths. If instead we encounter quiescent periods, we might consider profiling less frequently and thereby conserving battery life. Our ultimate objective is to treat FCS floats as expendable.

PRE-DEFINED PARAMETERS

$N_{\mathrm{seg}} = 512$, $N_{\mathrm{fft}} = 256$, $f_{\mathrm{l}}, f_{\mathrm{m}}, f_{\mathrm{h}} = 1, 3, 5\,\mathrm{Hz}$, $C_{2P} = 77\,\mathrm{psi\,V^{-1}}$ (Appendix B)

ONBOARD CALCULATIONS

Reshape raw voltage signals
Convert each 1D signal to a 2D array ($N_{\mathrm{blk}}, N_{\mathrm{seg}}$)

Discard non-profiling data
Use W_{min} threshold ($\propto \min|\Delta V_P(t_i)|$, Eq. 14, Appendix B)

Record *T* and *P* voltage quantities for each block
$\langle V_{T1}\rangle, \langle V_{T2}\rangle, V_P(N_{\mathrm{seg}})$

Despike shear voltages
Apply 3σ threshold to V_{s1} and V_{s2} (Appendix E)

Calculate voltage spectra
$\Psi_{s1}(f), \Psi_{s2}(f), \Psi_{Tt1}(f)$, and $\Psi_{Tt2}(f)$

Fit shear spectra over two ranges

$\sum_f f^{1/3}\Psi_{s1}(f)/\sum_f f^{2/3}$	over f_{l}–f_{m}	(Eq. 24)
—"— —"—	over f_{m}–f_{h}	
$\sum_f f^{1/3}\Psi_{s2}(f)/\sum_f f^{2/3}$	over f_{l}–f_{m}	
—"— —"—	over f_{m}–f_{h}	

Fit *Tt* spectra over two ranges

$\sum_f f^{1}\Psi_{Tt1}(f)/\sum_f f^{2}$	over f_{l}–f_{m}	(Eq. 34)
—"— —"—	over f_{m}–f_{h}	
$\sum_f f^{1}\Psi_{Tt2}(f)/\sum_f f^{2}$	over f_{l}–f_{m}	
—"— —"—	over f_{m}–f_{h}	

POST-PROCESSING

Calibrate averaged voltages
T_1 and T_2 (Eq. 6), P (Eq. 12), and W (Eq. 13)

Derive viscosity and thermal diffusivity
Use measured T and P together with S from SOLO-II CTD

Calculate four 'initial' turbulent dissipation values
For S_1 and S_2, get $\varepsilon_{\mathrm{init}}$ for f_{l}–f_{m} and f_{m}–f_{h} (Eq. 24)

Repeat step above for thermal dissipation
For Tt_1 and Tt_2, get χ_{init} for f_{l}–f_{m} and f_{m}–f_{h} (Eq. 34)

Calculate the correction factors
F_{Na} (Eq. 21) and F_{Kr} (Eq. 31)

Correct initial estimates
$\varepsilon_{\mathrm{init}} \rightarrow \varepsilon$ (Eq. 17) and $\chi_{\mathrm{init}} \rightarrow \chi$ (Eq. 30)

Combine f_{l}–f_{m} and f_{m}–f_{h} fit values
ε (Eqs. 25 and 27) and χ (Eq. 35)

Calculate goodness of fit of spectra
ε fit score (Eq. 26) and χ fit score (Eq. 36)

Figure 11. Summary of the data reduction scheme. Each 512-element segment of data is ultimately compressed down to the ~~15~~ 12 highlighted quantities that are then transmitted. These are calibrated and/or converted into turbulence quantities in post-processing.

Appendix A: Transfer functions for FCS sensors

Voltage signals from shear probes and thermistors are a smoothed representation of the true environmental signal. If the smoothing is a spatial effect, it is described by a transfer function $H^2(k)$. If the smoothing is a temporal effect, it is more natural to use $H^2(f)$. We can use these interchangeably because $f = Wk$ and therefore $H^2(f) = H^2(Wk)$. For FCS, there are three components to the transfer function for each sensor:

$$H_s^2(k) = H_{\rm SP}^2(k)\, H_{\rm AA}^2(f)\, H_{\rm D}^2(f) \tag{A1}$$

$$H_{Tt}^2(k) = H_{\rm FT}^2(f)\, H_{\rm AA}^2(f)\, H_{\rm D}^2(f) \tag{A2}$$

where we have used the following shorthand: SP = shear probe, FT = fast thermistor, AA = anti-aliasing, and D = digital. We describe each of these in turn.

Shear probes built and calibrated by the Ocean Mixing Group are very close in dimension to those examined by Ninnis (1984) who measured their wavenumber response and represented it as

$$H_{\rm SP}^2(k) = \sum_{n=0}^{4} a_n \left(\frac{k}{k_0}\right)^n \tag{A3}$$

where $a_0 = 1.000$, $a_1 = -0.164, a_2 = -4.537, a_3 = 5.503$, $a_4 = -1.804$, and $k_0 = 170\,\text{cpm}$.

Temporal averaging of temperature at high frequencies due to the thermal response of the fast thermistor is modeled ~~following Sommer et al. (2013) and Lien et al. (2016)~~using a double-pole filter:

$$H_{\rm FT}^2(f) = \frac{1}{\left(1+(2\pi f\tau)^2\right)^2}\,\frac{1}{\left(1+(f/f_{\rm c})^2\right)^2} \tag{A4}$$

where ~~$\tau = 0.01$~~the cut-off frequency $f_{\rm c} = 30$ ~~s so that $H_{\rm FT}^2(5\,\text{Hz}) = 0.83$. Note that there is large sensor-to-sensor variation among thermistors, which means there is not one true thermal response correction (Nash et al. 1999) .Compared to Sommer et al. (2013), other nominal corrections tend to be less aggressive (see, e.g., Bluteau et al. 201 . Our reduced scheme is built in such a way that a different correction can be applied in post-processing if desired~~Hz. This comes from Nash et al. (1999), who measured the frequency response for two different thermistors on an instrument profiling at $0.3\,\text{m}\,\text{s}^{-1}$ and found cut-off frequencies of 25.1 and 36.7 Hz (see their Fig. A2). The 30 Hz value is the approximate mean of these two values.

Raw shear and thermistor voltage signals are both subject to two filters. First, an analog antialiasing filter (two-pole Butterworth) with an $f_c = 40$ Hz cut-off:

$$H_{AA}^2(f) = \frac{1}{1+(f/f_c)^4}. \tag{A5}$$

After the analog signal is anti-aliased, it is digitized at 400 Hz. Before subsampling to the final 100 Hz output, the signal is digitally filtered. For the 2019 FCS cruise, the signal was convolved with a symmetric 29-element kernel in which the first 15 elements were

$$g_i = (2^{16}-1)^{-1} \times [52, 221, 393, 427, 174, 0, 0, 0, 0, 0, \\ 1970, 5054, 8202, 10558, 11433]. \tag{A6}$$

This is a sinc kernel but with negative values set to zero. (We are currently investigating better choices for future implementations). The filter has a half-power (-3 db) point at 25 Hz.

Appendix B: Identifying the start and end of a profile

Early in our processing routine, we partition the raw voltage signals into 512-element segments. In order to discard the segments in which FCS was not profiling, we need robust (yet simple) criteria that demarcate the start and end of a profile. For the start, we search for the first three consecutive segments in which $W_{\min} > 0.05\,\mathrm{m\,s^{-1}}$. For the end, we swap the inequality.

A drawback of this approach is the appearance of a quantity in physical units ($0.05\,\mathrm{m\,s^{-1}}$). This is the one instance where we hard code a calibration coefficient in the onboard software, rather than apply it in post-processing. Fortunately, the relevant coefficient can be approximated as constant: $C_{2P} = 76.7\,\mathrm{psi\,V^{-1}}$ (barring a redesign of the circuitry or the use of a different brand or model of pressure sensor). For the two units already built, $C_{2P} = 76.81\,\mathrm{psi\,V^{-1}}$ and $76.53\,\mathrm{psi\,V^{-1}}$. By comparison, among the four shear probes on the two units, the calibration coefficients vary by 30%.

At least for the initial implementation of our scheme, we do not include an algorithm to detect the surface to within centimeters. Doing so would let us work backward to put our uppermost depth bin as close to the surface as possible. However, we expect that this could be a fragile part of the scheme. Further, FCS lacks a micro-conductivity sensor, which is likely the sensor best suited for identifying the air–sea interface (e.g., Ward et al. 2014).

Without surface detection, the depths of the uppermost bins will be realized randomly. In the worst cases, we would discard the top $\sim$1 m (5 s at $\sim$0.2 m s^{-1}). To alleviate this, we may use half-overlapping bins near the surface. The exact implementation will be determined later in the development.

Appendix C: Least-squares fitting of power laws

In this paper, we use power law fits to derive turbulence quantities: $\Psi_s = A_\varepsilon f^{1/3}$ and $\Psi_{Tt} = A_\chi f^1$, where A_ε and A_χ are substitutes for the expressions in Eqs. 23 and 33. With only a single parameter for each fit, implementing a least-squares fit is easy.

Assume we are fitting the vector Ψ_i to the function Af_i^n where n is either $1/3$ or 1. The sum of squared residuals is therefore

$$\sum r_i^2 = \sum (\Psi_i - Af_i^n)^2 . \tag{C1}$$

The minimum with respect to A is where the derivative is zero:

$$\frac{\partial}{\partial A} \sum r_i^2 = \sum -2f_i^n (\Psi_i - Af_i^n) = 0. \tag{C2}$$

Hence,

$$A = \frac{\sum f_i^n \Psi_i}{\sum f_i^{2n}}. \tag{C3}$$

We had originally intended to find A by following Becherer and Moum (2017), who were fitting $f^{1/3}$ spectra. Their simpler method, $A = \sum(\Psi_i / f_i^n)$, is equivalent to a least-squares fit except that the quantity minimized is the sum of the squares of the *adjusted* residuals, where adjusted means divided by f^n. Differences can be ignored when $n = 1/3$, but not when $n = 1$.

Appendix D: Standard processing of FCS turbulence measurements

The standard processing of FCS turbulence data differs from the reduced scheme in three ways. First, raw data are despiked differently (Appendix E). Second, the 100 Hz raw voltage signals are calibrated into physical quantities right away. Hence, means and spectra are calculated in physical units, not voltage units. Third, the integration of spectra occurs over a variable wavenumber band, which is found iteratively.

When integrating shear spectra (after correction; Appendix A) to find ε, we follow the approach used for the Chameleon profiler (Moum et al. 1995). A first estimate of ε is made by integrating over $k = 4$–10 cpm. This value provides a first estimate of the Kolmogorov wavenumber $k_s = (\varepsilon/\nu^3)^{1/4}/2\pi$. (The lower limit for Chameleon is 2 cpm, but we increase this for FCS given its slower profiling speed and hence the possibility of contamination by waves at lower wavenumbers.) The upper integral limit is then set to $0.5k_s$ (with a minimum of 10 cpm and a maximum of 45 cpm). The Nasmyth spectra (Eq. (15)) is integrated over the same wavenumber range. If the measured and Nasmyth integrals are within 1%, then ε is set equal to the integral of the Nasmyth spectrum over all k. Otherwise, ε and k_s are adjusted iteratively until the two integrals agree.

A similar approach is used for integrating T_t spectra to find χ. The model spectrum is the Kraichnan spectrum (Eq. (28)) and, again, the lower limit of integration is 4 cpm. The upper limit is the Batchelor wavenumber $k_b = (\varepsilon/\nu D_T^2)^{1/4}/2\pi$ (with a maximum defined by $kW = 15$ Hz).

Appendix E: Identifying and removing noise and spikes in the shear signals

To properly despike the raw output of a shear probe requires several steps. Lueck et al. (2018) describe a process in which the signal is high-passed, then rectified, and then low-passed to derive a measure of the local variance. A value is defined as a spike if it is more than eight times (or similar threshold) above the local variance. Spikes are replaced with an average based on surrounding points. This process is then repeated on the new signal, and so on until no spikes are identified.

In our standard processing of FCS data, we use the Lueck et al. (2018) despiking routine. For our data reduction scheme, we use an approach that is easier to implement and quicker to compute, albeit less precise. For each 512-element segment of data, a spike is defined as any data point larger than three standard deviations from the mean. These spikes are replaced by the mean of remaining values in the segment.

Code availability. Our Matlab implementation of the processing code is available from github.com/OceanMixingGroup/flippin-chi-solo.

Data availability. Raw and processed data for the 2019 experiment are available at doi.org/10.5281/zenodo.5719505 or kghughes.com/data.

Author contributions. KGH designed the reduction scheme and led the writing of the paper. All authors contributed to the final version. JNM and DLR lead the development of the FCS profiler on which much of the paper is based.

Competing interests. The authors declare that they have no conflict of interest.

Acknowledgements. This work was funded by the Office of Naval Research under grant N00014-17-1-2700 (OSU) and N00014-17-1-2762 (SIO) and continued as part of the ARCTERX (Island Arc Turbulent Eddy Regional Exchange) program under grants N00014-21-1-2878 (OSU), N00014-21-1-2762, and N00014-21-1-2747 (SIO). Engineers who contributed to the design and construction of FCS and its sensors: Craig Van Appledorn, Kerry Latham, Pavan Vutukur, Mark Borgerson (all from OSU) and Ben Reineman, Kyle Grindley, Jeff Sherman from SIO. Aurélie Moulin executed initial turbulence processing, and Emily Shroyer provided many helpful comments on early drafts. ~~Reviews from two anonymous reviewers helped improve many aspects of this paper~~Thanks to the reviewers including Cynthia Bluteau and Toshiyuki Hibiya.

References

Becherer, J. and Moum, J. N.: An efficient scheme for onboard reduction of moored χpod data, J. Atmos. Oceanic Technol., 34, 2533–2546, https://doi.org/10.1175/JTECH-D-17-0118.1, 2017.

Bluteau, C. E., Jones, N. L., and Ivey, G. N.: Estimating turbulent kinetic energy dissipation using the inertial subrange method in environmental flows, Limnol. and Oceanogr. Methods, 9, 302–321, https://doi.org/10.4319/lom.2011.9.302, 2011.

Bluteau, C. E., Jones, N. L., and Ivey, G. N.: Estimating turbulent dissipation from microstructure shear measurements using maximum likelihood spectral fitting over the inertial and viscous subranges, J. Atmos. Oceanic Technol., 33, 713–722, https://doi.org/10.1175/JTECH-D-15-0218.1, 2016.

Bluteau, C. E., Lueck, R. G., Ivey, G. N., Jones, N. L., Book, J. W., and Rice, A. E.: Determining mixing rates from concurrent temperature and velocity measurements, J. Atmos. Oceanic Technol., 34, 2283–2293, https://doi.org/10.1175/JTECH-D-16-0250.1, 2017.

Goodman, L., Levine, E. R., and Lueck, R. G.: On measuring the terms of the turbulent kinetic energy budget from an AUV, J. Atmos. Oceanic Technol., 23, 977–990, https://doi.org/10.1175/JTECH1889.1, 2006.

Greenan, B. J. W., Oakey, N. S., and Dobson, F. W.: Estimates of dissipation in the ocean mixed layer using a quasi-horizontal microstructure profiler, J. Phys. Oceanogr., 31, 992–1004, https://doi.org/10.1175/1520-0485(2001)031<0992:EODITO>2.0.CO;2, 2001.

Kraichnan, R. H.: Small-scale structure of a scalar field convected by turbulence, Phys. Fluids, 11, 945–953, https://doi.org/10.1063/1.1692063, 1968.

Levine, E. R. and Lueck, R. G.: Turbulence measurement from an autonomous underwater vehicle, J. Atmos. Oceanic Technol., 16, 1533–1544, https://doi.org/10.1175/1520-0426(1999)016<1533:TMFAAU>2.0.CO;2, 1999.

Lien, R.-C., Sanford, T. B., Carlson, J. A., and Dunlap, J. H.: Autonomous microstructure EM-APEX floats, Methods Oceanogr., 17, 282–295, https://doi.org/10.1016/j.mio.2016.09.003, 2016.

Lueck, R.: Calculating the rate of dissipation of turbulent kinetic energy, Tech. rep., Rockland Scientific, https://rocklandscientific.com/support/knowledge-base/technical-notes/, 2013.

Lueck, R., Murowinski, E., and McMillan, J.: A guide to data processing: ODAS Matlab library v4.3., Tech. rep., Rockland Scientific, https://rocklandscientific.com/support/knowledge-base/technical-notes/, 2018.

Lueck, R. G., Wolk, F., and Yamazaki, H.: Oceanic velocity microstructure measurements in the 20th century, J. Oceanogr., 58, 153–174, https://doi.org/10.1023/A:1015837020019, 2002.

Merckelbach, L. M. and Carpenter, J. R.: Ocean glider flight in the presence of surface waves, J. Atmos. Oceanic Technol., 38, 1265–1275, https://doi.org/10.1175/JTECH-D-20-0206.1, 2021.

Moum, J. N.: Ocean speed and turbulence measurements using pitot-static tubes on moorings, J. Atmos. Oceanic Technol., 32, 1400–1413, https://doi.org/10.1175/JTECH-D-14-00158.1, 2015.

Moum, J. N. and Nash, J. D.: Mixing measurements on an equatorial ocean mooring, J. Atmos. Oceanic Technol., 26, 317–336, https://doi.org/10.1175/2008JTECHO617.1, 2009.

Moum, J. N., Gregg, M. C., Lien, R. C., and Carr, M. E.: Comparison of turbulence kinetic energy dissipation rate estimates from two ocean microstructure profilers, J. Atmos. Oceanic Technol., 12, 346–366, https://doi.org/10.1175/1520-0426(1995)012<0346:COTKED>2.0.CO;2, 1995.

Moum, J. N., Rudnick, D. L., Shroyer, E. L., Hughes, K. G., Reineman, B. D., Grindley, K., Sherman, J., Vutukur, P., Van Appledorn, C., Latham, K., Moulin, A. J., and Johnston, T. M. S.: Flippin' χSOLO, an upper ocean autonomous turbulence profiling float, J. Atmos. Oceanic. Tech, under review.

Nash, J. D., Caldwell, D. R., Zelman, M. J., and Moum, J. N.: A thermocouple probe for high-speed temperature measurement in the ocean, J. Atmos. Oceanic Technol., 16, 1474–1482, https://doi.org/10.1175/1520-0426(1999)016<1474:ATPFHS>2.0.CO;2, 1999.

Nasmyth, P. W.: Oceanic turbulence, Ph.D. thesis, Univ. British Columbia, https://doi.org/10.14288/1.0302459, 1970.

Ninnis, R.: The effects of spatial averaging on airfoil probe measurements of oceanic velocity microstructure, Ph.D. thesis, University of British Columbia, https://doi.org/10.14288/1.0053131, 1984.

Oakey, N. S.: Determination of the rate of dissipation of turbulent energy from simultaneous temperature and velocity shear microstructure measurements, J. Phys. Oceanogr., 12, 256–271, https://doi.org/10.1175/1520-0485(1982)012<0256:DOTROD>2.0.CO;2, 1982.

Osborn, T. R.: Vertical profiling of velocity microstructure, J. Phys. Oceanogr., 4, 109–115, https://doi.org/10.1175/1520-0485(1974)004<0109:VPOVM>2.0.CO;2, 1974.

Peterson, A. K. and Fer, I.: Dissipation measurements using temperature microstructure from an underwater glider, Methods Oceanogr., 10, https://doi.org/10.1016/j.mio.2014.05.002, 2014.

Rainville, L., Gobat, J. I., Lee, C., and Shilling, G.: Multi-month dissipation estimates using microstructure from autonomous underwater gliders, Oceanography, 30, 49–50, https://doi.org/10.5670/oceanog.2017.219, 2017.

Roemmich, D., Riser, S., Davis, R., and Desaubies, Y.: Autonomous profiling floats: Workhorse for broad-scale ocean observations, Mar. Technol. Soc. J., 38, 21–29, https://doi.org/10.4031/002533204787522802, 2004.

Roemmich, D., Alford, M. H., Claustre, H., Johnson, K., King, B., Moum, J., Oke, P., Owens, W. B., Pouliquen, S., Purkey, S., Scanderbeg, M., Suga, T., Wijffels, S., Zilberman, N., Bakker, D., Baringer, M., Belbeoch, M., Bittig, H. C., Boss, E., Calil, P., Carse, F., Carval, T., Chai, F., Conchubhair, D., d'Ortenzio, F., Dall'Olmo, G., Desbruyeres, D., Fennel, K., Fer, I., Ferrari, R., Forget, G., Freeland, H., Fujiki, T., Gehlen, M., Greenan, B., Hallberg, R., Hibiya, T., Hosoda, S., Jayne, S., Jochum, M., Johnson, G. C., Kang, K., Kolodziejczyk, N., Körtzinger, A., Traon, P.-Y. L., Lenn, Y.-D., Maze, G., Mork, K. A., Morris, T., Nagai, T., Nash, J., Garabato, A. N., Olsen, A., Pattabhi, R. R., Prakash, S., Riser, S., Schmechtig, C., Schmid, C., Shroyer, E., Sterl, A., Sutton, P., Talley, L., Tanhua, T., Thierry, V., Thomalla, S., Toole, J., Troisi, A., Trull, T. W., Turton, J., Velez-Belchi, P. J., Walczowski, W., Wang, H., Wanninkhof, R., Waterhouse, A. F., Waterman, S., Watson, A., Wilson, C., Wong, A. P. S., Xu, J., and Yasuda, I.: On the future of Argo: A global, full-depth, multi-disciplinary array, Front. Mar. Sci., 6, 439, https://doi.org/10.3389/fmars.2019.00439, 2019a.

Roemmich, D., Sherman, J. T., Davis, R. E., Grindley, K., McClune, M., Parker, C. J., Black, D. N., Zilberman, N., Purkey, S. G., Sutton, P. J. H., and Gilson, J.: Deep SOLO: A Full-Depth Profiling Float for the Argo Program, J Atmos. Oceanic Technol., 36, 1967–1981, https://doi.org/10.1175/JTECH-D-19-0066.1, 2019b.

Ruddick, B., Anis, A., and Thompson, K.: Maximum likelihood spectral fitting: The Batchelor Spectrum, J. Atmos. Oceanic Technol., 17, 1541–1555, https://doi.org/10.1175/1520-0426(2000)017<1541:MLSFTB>2.0.CO;2, 2000.

Sanchez, X., Roget, E., Planella, J., and Forcat, F.: Small-scale spectrum of a scalar field in water: The Batchelor and Kraichnan models, J. Phys. Oceanogr., 41, 2155–2167, https://doi.org/10.1175/JPO-D-11-025.1, 2011.

Shroyer, E. L., Rudnick, D. L., Farrar, J. T., Lim, B., Venayagamoorthy, S. K., St. Laurent, L. C., Garanaik, A., and Moum, J. N.: Modification of upper-ocean temperature structure by subsurface mixing in the presence of strong salinity stratification, Oceanography, 29, https://doi.org/10.5670/oceanog.2016.39, 2016.

Sommer, T., Carpenter, J. R., Schmid, M., Lueck, R. G., and Wüest, A.: Microstructure sensor responses with implications for double-diffusive fluxes, J. Atmos. Oceanic Technol., 30, 1907–1923, https://doi.org/10.1175/JTECH-D-12-00272.1, 2013.

Ward, B., Fristedt, T., Callaghan, A. H., Sutherland, G., Sanchez, X., Vialard, J., and ten Doeschate, A.: The Air–Sea Interaction Profiler (ASIP): An autonomous upwardly rising profiler for microstructure measurements in the upper ocean, J. Atmos. Oceanic Technol., 31, 2246–2267, https://doi.org/10.1175/JTECH-D-14-00010.1, 2014.